

1 **Constraining the timing and processes of pediment formation and** 2 **dissection: implications for long-term evolution in the Western Cape,** 3 **South Africa**

4 Janet C. Richardson¹, Veerle Vanacker², David M. Hodgson³, Marcus Christl⁴, Andreas Lang⁵

5 ¹Geography and Geology: Department of History, Geography and Social Sciences, Edge Hill University, Ormskirk, L39 4QP,
6 UK

7 ²Earth and Life Institute, Centre for Earth and Climate Research, Université catholique de Louvain, Louvain-la-Neuve,
8 1348, Belgium

9 ³School of Earth and Environment, University of Leeds, Leeds, LS2 9JT, UK

10 ⁴Ion Beam Physics, ETH Zürich, Zürich, Otto-Stern-Weg 5, CH 8093, Switzerland

11 ⁵Department of Geography and Geology, Universität Salzburg, Salzburg, A-5020, Austria

12

13 *Correspondence to:* Janet C. Richardson (Janet.Richardson@edgehill.ac.uk)

14 **Abstract.** Pediment surfaces are a widespread feature of the southern African landscape and have long been regarded as ancient
15 landforms. Cosmogenic nuclide data from four pediment surfaces in the Gouritz catchment, Western Cape, South Africa are
16 reported, including boulder surface samples and a depth profile through a colluvial pediment deposit. [Pediment surfaces are](#)
17 [remarkably stable with long-term denudation rates between 0.3 and 1.0](#) ~~The results indicate low surface lowering rates (0.315~~
18 ~~to 0.954 m My⁻¹, and their ¹⁰Be concentrations approach or at secular equilibrium.) and minimum exposure ages of 0.678–~~
19 ~~4.462 My (assuming denudation rates of 0.3 m My⁻¹).~~ Duricrusts have developed in the pediments and are preserved in some
20 locations, which represent an internal geomorphic threshold limiting denudation and indicate at least ~~1.2~~ My of geomorphic
21 stability following pediment formation. The pediments and the neighbouring Cape Fold Belt are deeply dissected by small
22 order streams that form up to 280 m deep river valleys in the resistant fold belt bedrock geology, indicating a secondary incision
23 phase of the pediments by these smaller order streams. Using the broader stratigraphic and geomorphic framework, the
24 minimum age of pediment formation is considered to be Miocene. Several pediment surfaces grade above the present trunk
25 valleys of the Gouritz River, which suggests that the trunk rivers are long-lived features that acted as local base levels during
26 pediment formation and later incised pediments to present levels. The geomorphic processes controlling the formation and
27 evolution of the pediments varied over time; with pediments formed by hillslope diffusive processes as shown by the lack of
28 fluvial indicators in the colluvial deposits and later development by fluvial processes with small tributaries dissecting the
29 pediments. Integrating various strands of evidence indicates that the pediments are long-lived features. [Caution should be taken](#)
30 [when interpreting cosmogenic nuclide ages from pediment surfaces in ancient landscapes, as isotopic steady state conditions](#)
31 [can be reached.](#)

32

Formatted: Not Highlight

Formatted: Superscript, Not Highlight

Formatted: Not Highlight

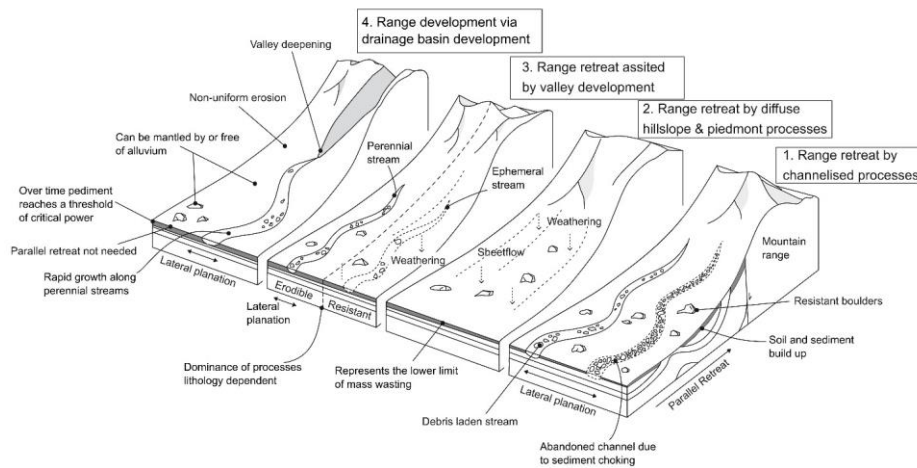
33 **1 Introduction**

34

35 Recent advancements in geochronology allow erosion rates and exposure ages of landforms to be established, and to place
36 more precise constraints on landscape evolution. Establishing erosion rates and landform ages is essential for linking the
37 evolution of drainage systems to downstream aggradation processes (e.g. Gallagher and Brown, 1999; Chappell et al., 2006;
38 Tinker et al., 2008a; Wittmann et al., 2009; Sømme et al., 2011; Romans et al., 2016), constraining surface uplift and tectonic
39 processes (e.g., Brook et al., 1995; Burbank et al., 1996; Granger et al., 1997; Jackson et al., 2002; Wittmann et al., 2007;
40 Bellin et al., 2014; Vanacker et al., 2015), and palaeo-climate reconstructions (e.g., Margerison et al., 2005; Dunai et al., 2005;
41 Owen et al., 2005; Willenbring and Blackenburg, 2010). Reconstructing ancient landforms and landscape development is
42 challenging due to fragmented preservation and increasing signal overprinting forming a landscape palimpsest (e.g. Chorley
43 et al., 1984; Bloom, 2002; Bishop, 2007; Jerolmack and Paola, 2010; Richardson et al., 2016). However, ancient landscapes
44 and landforms cover a large portion of the globe (e.g., (1) Australia – e.g., Ollier, 1991, Ollier and Pain, 2000, Twidale, 2007
45 a,b; (2) southern South Africa – e.g., Du Toit, 1954, King 1956a, (3) South America – e.g. King, 1956b, Carignano et al., 1999,
46 Demoulin et al., 2005, Panario et al., 2014, Peulvast and Bétard, 2015; (4) Asia – e.g., Gorelov et al., 1970, Gunnell et al.,
47 2007, Vanacker et al., 2007; and (5) Europe – e.g., Lidmar-Bergström, 1988, Bessin et al., 2015) and offer important insights
48 into long-term Earth surface dynamics and landscape evolution (indicating variation in erosion and deposition). Further,
49 pediments and planation surfaces can offer insights into mantle dynamics as they are characterised by undulations with middle
50 (several tens of kms) to very long wavelengths (several thousands of kms) characteristic of lithospheric and mantle
51 deformations (e.g., Braun et al., 2014; Guillocheau et al. 2018).

52

53 The formation of pediments is contentious and four categories of landscape evolution models (Fig.1) exist that address the
54 evolution of pediments and surrounding mountain belts (Dohrenward and Parsons, 2009) (1) range front retreat where
55 channelised fluvial processes are dominant (e.g., Gilbert, 1877; Paige, 1912; Howard 1942); (2) range front retreat where
56 diffuse hillslope and ~~peidmont~~[pedmont](#) processes are dominant (e.g., Lawson, 1915; Rich; 1935; Kesel, 1977; Bourne and
57 Twidale, 1998; Dauteuil et al., 2015); (3) range front retreat as a result of fluvial and diffusive erosion processes (e.g., Bryan,
58 1923; Sharp, 1940); and (4) lowering of the range due to channelised flow, catchment development and fluvial incision (e.g.,
59 Lustig, 1969; Parsons and Abrahams, 1984). Model type 1 ~~also~~ acknowledges the occurrence of diffusive processes and model
60 type 2 ~~acknowledges~~ the occurrence of channelised erosion processes, but ~~each model argues these are~~ [consider them as](#)
61 subsidiary formation processes (Gilbert, 1877; Rich, 1935; Howard, 1942). Model type 3 integrates fluvial and diffusive
62 erosion processes, and their relative importance depends on the geomorphic setting (Bryan, 1923; Sharp, 1940) with [a](#)
63 dominance of diffusive processes in regions with erosion-resistant bedrock lithologies, ephemeral streams, and ~~a~~-low range.
64 Model type 4 is associated with drainage basin development in the range, and does not require parallel retreat of the mountain
65 front to form the pediment surfaces (Lustig, 1969; Parsons and Abrahams, 1984).



67

68 **Figure 1: Pediment evolution models showing the range of processes that can shape pediments; 1) Range retreat by**
 69 **channelised processes adapted from Gilbert, (1877), Paige (1912) and Howard (1942); 2) Range retreat by diffuse**
 70 **hillslope and piedmont processes adapted from Lawson (1915), Rich (1935), Kesel (1977), Bourne and Twidale (1998)**
 71 **and Dauteuil et al. (2015); 3) Range retreat assisted by valley development adapted from Bryan (1923) and Sharp (1940)**
 72 **and; 4) Range development via drainage basin development adapted from Lustig (1969) and Parsons and Abrahams**
 73 **(1984).**
 74

75 The geomorphology of southern Africa has long intrigued earth scientists (Rogers, 1903; Davis, 1906; Dixey, 1944; King,
 76 1948, 1949, 1953). Fundamental questions related to long-term landscape development remain contentious, such as the
 77 mechanisms and timing of surface uplift (e.g., Gallagher and Brown, 1999, Brown et al., 2002, Tinker et al., 2008b, Kounov
 78 et al., 2009, Decker et al., 2013; Wildman et al. 2015; Wildman et al. 2017; Stanley et al. 2021) and the chronological
 79 framework of the main phases of landscape development (Du Toit, 1937, 1954; King, 1951; Burke, 1996; Partridge, 1998;
 80 Brown et al., 2002; Doucouré and de Wit, 2003; de Wit, 2007; Kounov et al., 2015). In-situ produced cosmogenic nuclides
 81 (CRN) can offer key information to unravel questions related to landscape development and evolution and have been applied
 82 to ancient landforms within southern Africa (Fleming et al. 1999; Cockburn et al., 2000; Bierman and Caffee, 2001; van der
 83 Wateren and Dunai, 2001; Kounov et al., 2007; Codilean et al., 2008; Dirks et al., 2010; Decker et al., 2011; Erlanger et al.,
 84 2012; Chadwick et al., 2013; Decker et al., 2013). However, studies based on in-situ produced cosmogenic studies, in the
 85 region south of the Great Escarpment are sparse (e.g., Scharf et al., 2013; Bierman et al., 2014; Kounov et al., 2015).

86

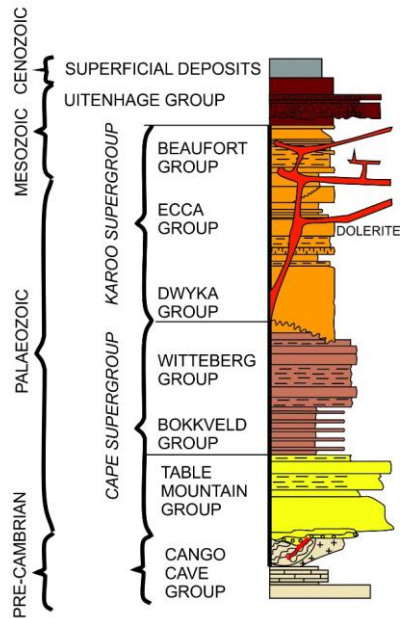
87 Pediments or erosional surfaces have been investigated in South Africa since the 1950's (King, 1953; King 1963; Partridge
88 and Maud, 1987), and have denudation rates that are an order of magnitude lower than those in other landforms within southern
89 Africa (van der Wateren and Dunai, 2001; Bierman et al., 2014; Kounov et al., 2015; Fig. 2). The pediment surfaces were
90 inferred as being early Cenozoic to Jurassic in age by King (1963). Large scale erosional features are also a feature of the
91 wider African continent, and extensive research has been undertaken to understand mantle dynamics associated with plateau
92 formation (e.g., Braun et al., 2014; Dauteuil et al., 2015; Guillocheau et al., 2015; Guillocheau et al., 2018). In this paper, we
93 present new isotopic data from pediment landforms in southern South Africa. The main aim of the paper is to constrain
94 landscape development using in-situ produced ¹⁰Be isotopes and to establish denudation rates and landform exposure ages.
95 The objectives of the paper are to: 1) assess the formative process associated with pediment evolution; 2) assess the cosmogenic
96 data within a wider geomorphic and geologic framework in order to test the performance of cosmogenic dating in a geomorphic
97 setting with very low denudation rates; and 3) discuss the implications for the wider landscape development of southern South
98 Africa.

99 2 Regional Setting

100 2.1 Geological setting

101 In the ~~area of study of~~ Western Cape, Southern Africa, the geology is dominated by strata of the Cape (Early Ordovician to
102 Early Carboniferous) and Karoo Supergroups (Late Carboniferous to Early Jurassic) (Johnson et al. 1995, Frimmel et al. 2001)
103 (Fig. 2), which are composed of various sandstone, siltstone and mudstone successions. Both supergroups have been subject
104 to low-grade burial metamorphism (Frimmel et al., 2001), with localised contact metamorphism during Jurassic dolerite
105 intrusion (Johnson et al.1995), and an estimated 6-7 km of exhumation during the Early Cretaceous (Tinker et al., 2008;
106 Wildman et al., 2015).~~Both supergroups have been metamorphosed, and the Karoo Supergroup has igneous intrusions.~~
107 Tectonic shortening during the latest Palaeozoic-to-early Mesozoic of the Cape and Karoo Supergroups of Cape and Karoo
108 Supergroups (Tankard et al. 2009; Hansma et al. 2016) have resulted in with E-W trending, northward verging, and eastward
109 plunging folds that decrease in amplitude northward and shorten northwards, and form the backbone of the exhumed Cape
110 Fold Belt (CFB)(Paton, 2006; Tinker et al., 2008b; Scharf et al., 2013; Spikings et al., 2015). During the Mesozoic, the rifting
111 of Gondwana initiated large-scale denudation across southern Africa. Using apatite fission track analyses of outcrop and
112 borehole samples, Tinker et al. (2008a) concluded that the southern Cape escarpment and coastal plain underwent 3.3 to 4.5
113 km of denudation since the Mid-Late Cretaceous and potentially 1.5 to 4 km within the Early Cretaceous, using a thermal
114 gradient of ~20°C/km. Wildman et al. (2015) processed 75 apatite fission track and 8 zircon fission track data from outcrop
115 and boreholes across the southwestern cape of South Africa (from coast to the escarpment). Using a thermal history-model and
116 a geothermal gradient of 22°C/km, they obtained an average of 4.5 km ~~of~~ denudation in the Mesozoic, since from the Late
117 Jurassic to the Early Cretaceous. However, their estimates range between 2.2 and 8.8 km of denudation using the upper and
118 lower ranges of the geothermal gradient and possible thermal histories bounded by 95% significance intervals, which provides

119 uncertainty on the inferred [exhumation](#) model. Richardson et al. (2017) used reconstructed geological cross sections [tied to](#)
 120 [apatite fission track data](#), and drainage reconstruction to model up to 4-11 km of denudation [across the Western Cape, with](#)
 121 [significant exhumation in the Early Cretaceous and lower amounts in the Late Cretaceous.](#)



126 **Figure 2: Stratigraphic chart showing the major lithostratigraphic units of [the Western Cape, South Africa.](#)**

127
 128 The mechanisms of regional uplift [during](#) since the Mesozoic, related to the anomalous height of southern Africa, are
 129 contentious; with landscape evolution either associated to mantle plumes (Nyblade and Robinson, 1994, Ebinger and Sleep,
 130 1998) or to plate tectonics, with uplift along flexures (Moore et al., 2009) [resulting in](#) and epeirogenic uplift (Brown et al.,
 131 1990). Furthermore, the occurrence and timing of later Cenozoic uplift is disputed (e.g., Brown et al., 2002; van der Beek et
 132 al., 2002). Burke (1996) proposed that the most recent uplift phase occurred ~30 Ma ago due to a thermal anomaly, [and](#) Green
 133 et al. (2016) also argued for Cenozoic uplift within southern South Africa that caused localised incision of the Gouritz River
 134 into the Swartberg mountain range. [However,](#) Partridge and Maud (1987) argued for two phases of uplift during the Neogene,

135 with a phase around 18 Ma and a more recent phase at 2.58 Ma. ~~Cenozoic uplift has been disputed by~~ Brown et al. (2002) and
136 ~~van der Beek et al. (2002) have questioned Cenozoic uplift~~ ~~-based on apatite fission track thermochronology, which does not~~
137 ~~have a signal for recent uplift.~~

138

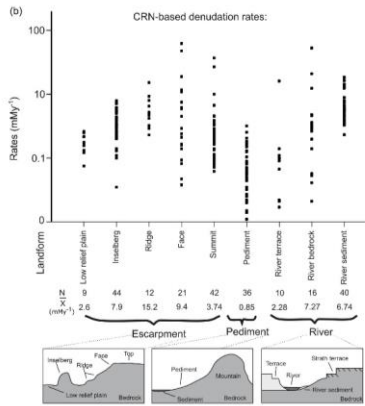
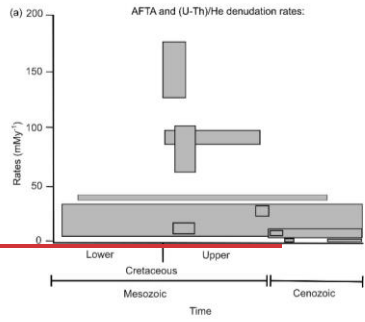
139 Figure 3 provides an overview of published geochronological studies in southern South Africa that used either apatite (U-
140 Th)/He and apatite fission track analysis to document landscape denudation from the Cretaceous to modern day, or in-situ
141 produced cosmogenic radionuclides (^{26}Al , ^{10}Be , ^3He , ^{21}Ne) to date landforms. Apatite (U-Th)/He and fission track data (Fig.
142 3) indicate high rates of denudation (up to 175 m My^{-1} , Tinker et al., 2008b) with respect to the present day rates, towards the
143 end of the Lower Cretaceous (100– 80 Ma) that decreased to up to 95 m My^{-1} by the late Cretaceous (90– 70 Ma; Brown et
144 al., 2002). Flowers and Schoene (2010) report negligible erosion since the Cretaceous, with rates as low as 5 m My^{-1} by the
145 late Eocene (36 My; Cockburn et al., 2000). Cosmogenic studies support low erosion rates within southern South Africa since
146 the start of the Cenozoic (Fig 3; Fleming et al., 1999; Cockburn et al., 2000; Bierman and Caffee, 2001; van der Wateren and
147 Dunai, 2001; Kounov et al., 2007; Codilean et al., 2008; Dirks et al., 2012; Decker et al., 2011; Erlanger et al., 2012; Chadwick
148 et al., 2013; Decker et al., 2013; Scharf et al., 2013; Bierman et al., 2014; Kounov et al., 2015). The majority of landforms are
149 eroding very slowly, with mean denudation rates ranging between 9.4 m My^{-1} for the escarpment faces to 0.85 m My^{-1} for
150 pediments (Fig. 3), although ~~one reported retreat rate of~~ 62.3 m My^{-1} ~~have has~~ been measured for ~~one~~ escarpment face retreat
151 (Fleming et al., 1999). In contrast, the Great Escarpment in the South African interior has higher fluvial incision rates than
152 southern South Africa: cosmogenic ^3He channel bed denudation rates range between 14 and 255 m My^{-1} and valley side and
153 valley top denudation rates range between 11 to 50 m My^{-1} for the Klip and Mooi Rivers and Schoonspruit, tributaries of the
154 Orange River (Keen-Zebert et al., 2016).

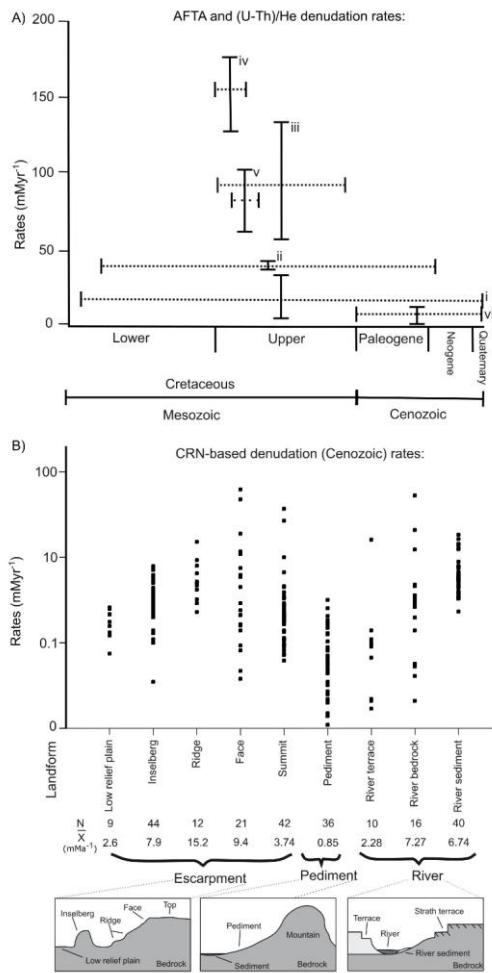
155

Formatted: Superscript

Formatted: Superscript

Formatted: Superscript





158 **Figure 3: Published exhumation and denudation rates for southern Africa. A) Apatite fission track and (U-Th)/He data**
159 **show large variation in exhumation rates since the Cretaceous, error bars show the range in exhumation rates and**
160 **integration timeframe, and include data from Gallagher and Brown, 1999 (i); Cockburn et al. 2000 (ii); Brown et al.**
161 **2002 (iii); Tinker et al. 2008b (iv); Kounov et al. 2009 (v) and; Flowers and Schoene, 2010 (vi). B) In-situ produced**
162 **cosmogenic (¹⁰Be, ²⁶Al, ²¹Ne and ³He) nuclide-derived denudation rates for escarpment, pediment and fluvial landforms.**
163 **Cosmogenic data is from the following sources; Flemming et al. 1999; Cockburn et al. 2000; Bierman and Caffee, 2001;**
164 **van der Wateren and Dunai, 2001; Kounov et al. 2007; Codilean et al. 2008; Dirks et al. 2012; Decker et al. 2011;**
165 **Erlanger et al. 2012; Chadwick et al. 2013; Decker et al. 2013; Scharf et al. 2013; Bierman et al. 2014; and Kounov et**
166 **al. 2015.**
167

168 Southern South Africa, below the Great Escarpment, is currently tectonically quiescent with only minor Quaternary-active
169 faults (Bierman et al., 2014) and low denudation and sediment production rates (Kounov et al., 2007; Scharf et al. 2013).
170 Minimum exposure ages for pediments range from 0.29 \pm 0.02 Ma (Bierman et al., 2014) to 5.18 \pm 0.18 Ma (Van der
171 Wateren and Dunai, 2001) with a mean minimum exposure age of 1.87 Ma (Pleistocene, van der Wateren and Dunai, 2001;
172 Bierman et al., 2014; Kounov et al., 2015).

173
174 The climate of southern South Africa has gradually moved towards more arid conditions since the Cretaceous (Partridge, 1997;
175 van Niekerk et al., 1999) with an abrupt change from humid/tropical to arid conditions at the end of the Cretaceous (Partridge
176 and Maud, 2000) as shown by silcrete formation and saline soils (Partridge and Maud, 1987). Although there is general
177 agreement about the overall aridification trend since the Cretaceous, several authors have argued that wetter phases occurred
178 from 65 – 30 Ma (Burke, 1996), or that the arid phase started as late as 18 Ma (Partridge and Maud, 1987). The **present**
179 **daypresent-day** climate of the Western Cape is primarily semi-arid (Dean et al., 1995), while the coastal region has a
180 Mediterranean type climate (Midgley et al., 2003).

181 2.2 Sample Sites

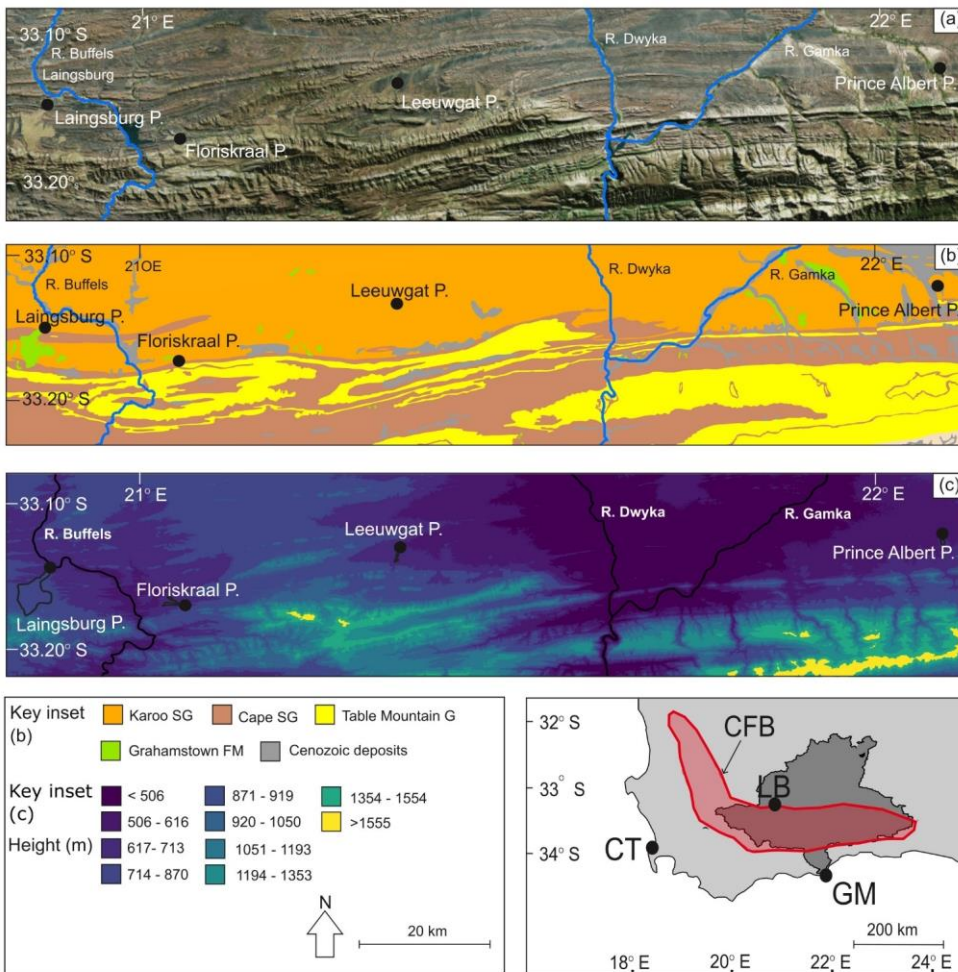
182 The sampling sites are located within the large antecedent Gouritz catchment (Fig. 4), where morphometric analysis has
183 identified the presence of flat surfaces or pediments that carry a thin sedimentary cover, hereafter called alluviated pediments
184 (<1m) (Richardson et al., 2016). The alluviated pediments grade away from the Cape Fold Belt (CFB) into adjacent alluvial
185 plains, and samples were collected from pediments on the northern flank of the Swartberg and Witteberg Mountains (CFB)
186 around Laingsburg, Floriskraal, Leeuwgat, and Prince Albert (Fig. 4a). Samples were taken from five deeply dissected
187 alluviated pediments ranging in surface area between < 1 to 20 km² and displaying slope angles below 10°, with most of the
188 slopes below 4° (Fig. 5).

Formatted: Superscript

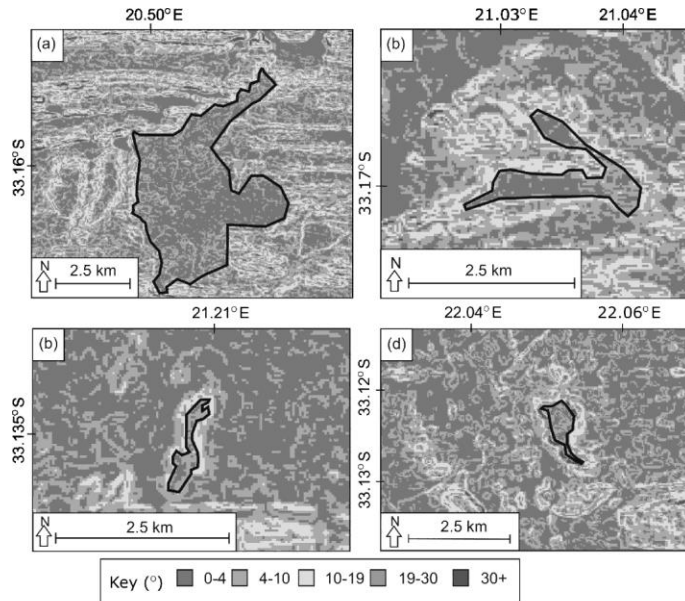
Formatted: Superscript

Formatted: Superscript

Formatted: Superscript



189
 190 **Figure 4: (a)** Pediment locations, the inset shows the location of the Gouritz catchment within South Africa, where CT
 191 – Cape Town, LB – Laingsburg; GM – Gouritzmond and the red polygon is the location of the Cape Fold Belt (CFB);
 192 (b) underlying geology below the pediments and; (c) pediment elevations (in m a.s.l.) as shown by elevation bins
 193 categorised by natural breaks in the elevation data. [Aerial imagery for \(a\) from ESRI, Geology information for \(b\)](#)
 194 [provided by the Geology Society of South Africa.](#)



196

197 **Figure 5: Pediment slope data (with slope given in °); (a) Laingsburg; (b) Floriskraal; (c) Leeuwgat and; (e) Prince**
 198 **Albert. For pediment locations please see Figure 4.**

199

200 The alluviated pediments are composed of unconsolidated, poorly-sorted gravel to boulder material in a matrix of sand (Fig.
 201 6) that unconformably overlie folded rocks of the Karoo Supergroup (Fig. 3b). Some pediments are capped by silcrete, calcrete
 202 or ferricrete (Helgren and Butzer, 1977; Summerfield, 1983; Marker and Holmes, 1999; Partridge, 1999; Partridge and Maud,
 203 2000; Marker et al., 2002). Ferricrete is dominant on the Laingsburg pediment. The silcrete is assigned to the Grahamstown
 204 Formation (Fig. 4b) that has poor age control (Mountain, 1980; Summerfield, 1983) due to the lack of formal identification of
 205 the extent of the silcretes. Electron spin resonance ages for two silcrete caps in the Kleine Karoo were dated at 7.3 and 9.4 Ma
 206 (Hagedorn, 1988).

207



208

209 **Figure 6: (a) Sedimentary log of the Laingsburg pediment showing the unsorted boulders (dominantly quartzite) to**
 210 **gravel size material; (b) photograph of the pediment and where the depth profile clasts were taken; (c) iron-rich**
 211 **palaeosol layer.**

212 3. Methodology

213 3.1 Cosmogenic radionuclide dating

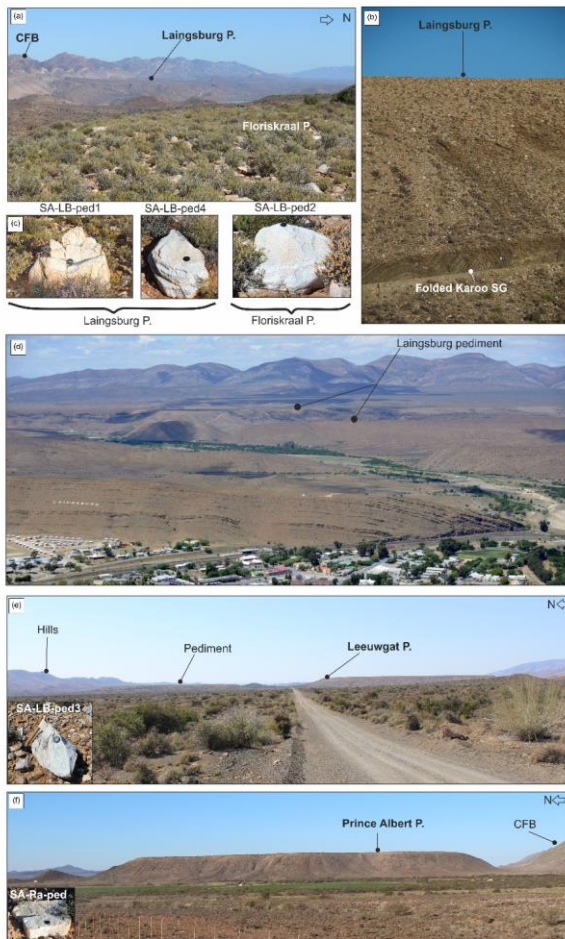
214 Two types of samples were collected for CRN analyses in 2014: five rock samples from alluviated pediment surfaces and

215 clasts from one depth profile in the Laingsburg pediment (Fig. 7, Table 1). Quartzite boulders from the Table Mountain

216 Group (Cape Supergroup) that were sampled at the surface of the pediments have a >1m diameter along their longest axis.

217 For the depth profile in the pediment, quartzite clasts (>25 cm diameter) were taken at the following depths (cm) below

218 ground level: 0, 30, 85, 150, 255 (Table 1).



219

220 **Figure 7: Sample sites; (a) Laingsburg pediment from the Floriskraal pediment; (b) Laingsburg pediment and**
 221 **contact with underlying folded Karoo Supergroup (SG) strata; (c) Boulder samples from Laingsburg and Floriskraal**
 222 **pediments; (d) large-scale picture of the Laingsburg pediment; (e) Leeuwgat pediment and boulder sample (inset); (f)**
 223 **Prince Albert and boulder sample (inset). The figure also shows the dissection of the pediments by small river**
 224 **catchments and how decoupled the Floriskraal and Prince Albert pediments are from the Cape Fold Belt.**

225 **Table 1: Site-specific information of the sampling sites for cosmogenic radionuclide analysis. All samples are taken**
 226 **from quartzite boulders, that were sampled either on the surface of the pediment (sample type = surf) or at depth**
 227 **(sample type = depth). The density of the sample or overburden (for depth samples) has been determined based on**
 228 **published density data of quartzite boulders and depth profiles in pediments by respectively Scharf et al. (2013) and**
 229 **Kounov et al. (2015).**

Sample ID	Sample type	Name	Latitude (°S)	Longitude (°E)	Elevation (m)	Density (g/cm ³)	Topographic Shielding	Cover correction
SA-PA_ped	Surf	Prince Albert	33.203	22.082	703	2.7	1.00	NA
SA-LB_ped1	Surf	Laingsburg	33.246	20.872	764	2.7	1.00	NA
SA-LB_ped2	Surf	Floriskraal	33.285	21.050	706	2.7	1.00	NA
SA-LB_ped3	Surf	Leeuwgat	33.221	21.347	691	2.7	1.00	NA
SA-LB_ped4	Surf	Laingsburg	33.261	20.854	791	2.7	1.00	NA
SA-LB_DP0	Depth	Laingsburg	33.256	20.851	776 9	1.6	0.99	NA
SA-LB_DP30	Depth	Laingsburg	33.256	20.851	776	1.6	0.99	0.73 9
SA-LB_DP85	Depth	Laingsburg	33.256	20.851	776	1.6	0.99	0.41 54
SA-LB_DP150	Depth	Laingsburg	33.256	20.851	776	1.6	0.99	0.21 37
SA-LB_DP255	Depth	Laingsburg	33.256	20.851	776	1.6	0.99	0.07 23

230

231 The samples were processed for in-situ cosmogenic ¹⁰Be following standard methods as described in von Blanckenburg (2004)
 232 and Vanacker et al. (2007). Rock samples were crushed, sieved and rock fragments of 250 to 500 μm diameter were selected
 233 for further lab processing. Quartz minerals were extracted by chemical leaching with a low concentration of acids (HCl, HNO₃,
 234 and HF) in an overhead shaker. Purified quartz samples were then leached with 24% HF for 1h to remove meteoric ¹⁰Be,
 235 followed by spiking the sample with 150 μg of ⁹Be and total decomposition in concentrated HF. The Beryllium in solution
 236 was extracted by ion exchange chromatography as described in von Blanckenburg et al. (1996). The ¹⁰Be/⁹Be ratios were
 237 measured using accelerator mass spectrometer on the 500 kV Tandy facility at ETH Zürich (Christl et al., 2013). Measured
 238 ¹⁰Be/⁹Be ratios were normalised to the ETH in-house secondary standard S2007N with a nominal ratio of 28.1×10⁻¹² (Kubik
 239 and Christl, 2010), which is in agreement with a ¹⁰Be half-life of 1.387 Ma (Chmeleff et al., 2010). Sample ratios were blank
 240 corrected ($7.54 \pm 9.67 \times 10^{-15}$) and the analytical uncertainties on the ¹⁰Be/⁹Be ratios of blanks and samples were then
 241 propagated into the 1σ analytical uncertainty for the ¹⁰Be concentrations (Table 2 and 3). Production rates were scaled
 242 following Dunai (2000) with a sea level high-latitude production rate of 4.28 atoms g_{qtz}⁻¹ yr⁻¹. The bulk density was set to 2.7
 243 g cm⁻³ for samples from quartzite boulders following Scharf et al. (2013), and to 1.6 g cm⁻³ for the overburden of the depth
 244 samples following earlier work on depth profiles in the Western Cape by Kounov et al. (2015). The concentrations were
 245 corrected for topographic shielding using the procedure described in Norton and Vanacker (2009).

246 **Table 2 : Cosmogenic nuclide data for a depth profile in Laingsburg. The reported ^{10}Be concentrations are corrected**
 247 **for procedural blanks, using a value of $7.54 \pm 9.67 \times 10^{-15}$, and the 1σ uncertainty estimates contain analytical errors**
 248 **from AMS measurement and blank error propagation.**
 249

Sample ID	Depth (cm)	^{10}Be concentration ($\pm 1\sigma$), ($\times 10^6$ at/g _{qtz})
SA-LB_DP0	0	5.460 ± 0.106
SA-LB_DP30	30	1.196 ± 0.111
SA-LB_DP85	85	0.893 ± 0.036
SA-LB_DP150	150	0.376 ± 0.016
SA-LB_DP255	255	0.133 ± 0.015

250

251

252 **Table 3: Cosmogenic nuclide data for surface samples from pediments. The reported ^{10}Be concentrations are corrected**
 253 **for procedural blanks, using a value of $7.54 \pm 9.67 \times 10^{-15}$, and the 1σ uncertainty estimates contain analytical errors**
 254 **from AMS measurement and blank error propagation. Maximum denudation rates and minimum durations of surface**
 255 **exposure were calculated using the CosmoCalc add-in for Excel (Vermeesch, 2007). For the surface exposure ages, we**
 256 **assumed (1) no erosion or burial since exposure, and (2) a maximum steady erosion rate of 0.3 m My^{-1} .**
 257

Sample ID	Location	^{10}Be concentration ($\times 10^6$ at/g _{qtz}) ($\pm 1\sigma$)	^{10}Be denudation rate (m My^{-1}) ($\pm 1\sigma$)	Minimum exposure age (Ma) ($\pm 1\sigma$)	
				No erosion or deposition	Erosion rate of 0.30 m My^{-1}
SA-PA_ped	Prince Albert	2.834 ± 0.055	0.954 ± 0.025	0.569 ± 0.010	0.678 ± 0.010
SA-LB_ped1	Laingsburg	5.199 ± 0.096	0.408 ± 0.013	1.131 ± 0.016	1.964 ± 0.016
SA-LB_ped2	Floriskraal	5.148 ± 0.095	0.383 ± 0.013	1.189 ± 0.016	2.220 ± 0.016
SA-LB_ped3	Leeuwgat	5.641 ± 0.103	0.315 ± 0.011	1.377 ± 0.018	4.462 ± 0.018
SA-LB_ped4	Laingsburg	4.252 ± 0.067	0.587 ± 0.014	0.848 ± 0.011	1.164 ± 0.010
SA-LB_DP0	Laingsburg	5.460 ± 0.106	0.373 ± 0.013	1.210 ± 0.018	2.333 ± 0.018

258

259

260 For the derivation of the minimum durations of exposure (Table 3), we used two different scenarios: a hypothetical case
 261 assuming no erosion or burial since exposure, and a second case assuming steady erosion of the pediment surface of 0.3 m My^{-1}

Formatted: Not Highlight

262 ¹ following Bierman et al. (2014). The CosmoCalc method, version 3.0 (Vermeesch, 2007) was employed to calculate
 263 maximum denudation rates and minimum surface exposure ages from the ¹⁰Be concentrations of the surface samples (Table
 264 3). The surface exposure ages are *minimum estimates* as isotopic steady state can be reached for old material.

265 In addition, we use a concentration depth profiling approach to better constrain the exposure and denudation of the Laingsburg
 266 area pediment. The accumulation of ¹⁰Be, $N_{total}(z,t)$, in the eroding surface of the pediments can be described as:

$$267 \quad N(z,t) = N_{inh}e^{-\lambda t} + \sum_i \frac{P_i(z)}{\lambda + \frac{\rho E}{\Lambda_i}} e^{-\rho(z_0 - Et)/\Lambda_i} \left(1 - e^{-\left(\lambda + \frac{\rho E}{\Lambda_i}\right)t} \right) \quad \text{Eq.1}$$

268 where E is expressed in cm/yr ($m \cdot My^{-1} \times 10^4$), t [yr] is the exposure age, λ [My^{-1}] the nuclide decay constant ($\lambda = \ln 2 / t_{1/2}$),
 269 z_0 (cm) the initial shielding depth ($z_0 = E \times t$), ρ [$g \cdot cm^{-3}$] the density of the overlying material, and Λ_i [g/cm²] the attenuation
 270 length. The production rate, $P_i(z)$ [atoms $\cdot g^{-1} \cdot yr^{-1}$], is a function of the depth, z [cm], below the surface. The subscript 'i'
 271 indicates the different production pathways of ¹⁰Be via spallation, muon capture and fast muons following Dunai (2010). In
 272 this study, the relative spallogenic and muogenic production rates are based on the empirical muogenic-to-spallogenic
 273 production ratios established by Braucher et al. (2011), using a fast muon relative production rate at SLHL of 0.87% and slow
 274 muon relative production rate at SLHL of 0.27%. The attenuation length was set to 152, 1500 and 4320 g cm⁻² for the
 275 production by, respectively, neutrons, negative muons and fast muons (Braucher et al., 2011). The depth profile is then solved
 276 numerically, based on a χ^2 -model fitting between the observed (Table 2) and simulated ¹⁰Be concentrations at
 277 different depths, for a wide range of exposure age (0.4 to 20 Ma), denudation rate (0 to 1.5 m My⁻¹), inheritance ($N_{inh}e^{-\lambda t} =$
 278 N_{255cm} vs. no inheritance) and deflation scenarios. The Nash-Sutcliffe efficiency and the chi-squared were used to assess the
 279 predictive power of the numerical models following Vandermaelen et al. (2022).

280 3.2 Morphometric Analysis

281 Aster 30m data was used to build a DEM of the study area in ArcGIS 10.1. The DEM was re-projected into WGS 1984 world
 282 Mercator coordinates and gaps were filled using the hydrology toolbox. The drainage was extracted using an upstream
 283 contributing area of 3.35 km², and both ephemeral and perennial streams were delineated (e.g., Abadelkaarem et al., 2012;
 284 Ghosh et al., 2014). Dissected pediments were derived using a method adapted from Bellin et al. (2014). The previous grading
 285 from the mountain front was reconstructed for each pediment in ArcGIS (Fig. 8). This surface was then placed into ArcScene
 286 10.1, with the difference between the reconstructed surface and the current topography (using the DEM) providing a minimum
 287 volume of material removed after pediment formation. A similar approach was applied to derive bulk erosion volumes for the
 288 small sub-catchments that back the pediment surfaces in the CFB. The bulk erosion is likely to be a minimum estimate of the
 289 total rock volume removed by erosion, as interfluvial erosion might have occurred (Bellin et al., 2014; Brocklehurst and
 290 Whipple, 2002). Eroded volumes were then converted to lithological thickness using the method of Aguilar et al. (2011).

Formatted: Superscript

Formatted: Superscript

Formatted: Superscript

Formatted: Subscript

Formatted: Superscript

Formatted: Superscript

Formatted: Not Highlight

Formatted: Not Highlight

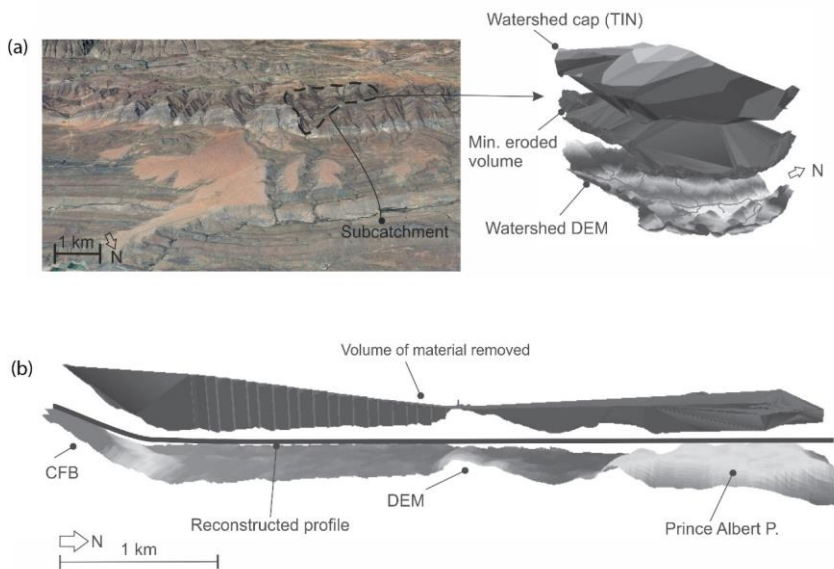
Formatted: Not Highlight

Formatted: Not Highlight

Formatted: Superscript, Not Highlight

Formatted: Not Highlight

Formatted: Not Highlight



291
 292 **Figure 8: Examples of (a) bulk eroded volumes from subcatchments and (b) cross section of the Prince Albert**
 293 **pediment showing the method used in ArcGIS for the volume of material removed around the pediment surface.**
 294 **[Imagery for \(a\) from © Google Earth 2015.](#)**

295 **4. Results**

296 **4.1 Alluviated pediment composition**

297 The contact with the underlying bedrock (e.g., Dwyka Group) is erosional and undulating, it is not a smooth planation contact.
 298 The alluviated pediments are composed of poorly sorted boulders to pebbles, with a matrix of sandy gravel. The clasts are
 299 predominantly quartzites (Table Mountain Group); however smaller clasts of Dwyka Group lithologies are present. Towards
 300 the top of the profile there is a small transition zone of gravel, which is capped by an iron crust (Fig. 6). There is no indication
 301 of fluvial activity (i.e., imbrication). There is no grading or sediment clast size variation throughout the profile, and the clasts
 302 range from sub-rounded to sub-angular.

303

304 4.2 Cosmogenic nuclides

305 The in-situ produced ^{10}Be concentrations in boulders The surface lowering rates (Table 3) calculated for the boulders sampled
306 on the pediment surface range between $(2.834 \pm 0.055) \times 10^6$ and $(5.641 \pm 0.103) \times 10^6$ at/g_{qtz} . The CRN concentrations are
307 indicative for old surfaces with show very low maximum denudation, and we obtained long-term denudation rates, which
308 range from of 0.315 to 0.954 m My^{-1} for the pediments. The alluviated pediment in the Prince Albert area has the highest rate
309 of maximum surface lowering (0.954 m My^{-1}), which is an order of magnitude higher than the average surface lowering rate
310 of the other studied alluviated pediments in the The Laingsburg area alluviated pediment Laingsburg area. In the latter area,
311 the surface denudation rates decrease from the CFB towards the proximal part of the pediment (Table 3).

312 has higher rates of surface lowering closer to the CFB, with denudation rates decreasing towards the proximal part of the
313 pediment as shown by the boulder samples. The alluviated pediment in the Prince Albert area has the highest rate of maximum
314 surface lowering (0.954 m My^{-1}), which is an order of magnitude higher than the average surface lowering rate of the other
315 studied alluviated pediments. The minimum exposure ages assuming no erosion or burial (Table 3) indicate that the
316 alluviated pediments are long-lived, and have been exposed for at least 0.678 to 4.461 My (when we assume that the surface
317 was lowered by 0.3 m My^{-1}). The CRN-depth profile in the Laingsburg Laingsburg pediment demonstrates the existence of a
318 deflation surface as result of differential erosion. The profile consists of 5 samples, taken at the surface, 30, 80, 150 and 255
319 cm depth. The ^{10}Be concentrations steadily decrease with depth (Fig. 9a), whereby the ^{10}Be concentration of four lower samples
320 decreases exponentially with depth, as theoretically expected for cosmogenic radionuclide production by neutrons with a fitted
321 exponent of -0.01 ($N_{10\text{Be}} \approx e^{-0.01 \times \text{depth}}$, $\text{RMSE} = 1.49 \times 10^5 \text{ at/g}_{\text{qtz}}$) corresponding well to an attenuation length of 160 g/cm^2
322 for a matrix density of 1.6 g/cm^3 . In contrast, the top sample (SA-LB-DP0) has a concentration that is more than double the
323 theoretically expected ^{10}Be concentration (Table 3). We attribute this phenomenon to surface deflation: boulders covering the
324 ground surface are part of a deflation amouing, and are longer exposed to cosmic rays than the matrix of sandy gravel in
325 which they are now embedded. Based on the exponential fit through the four lowermost data points, we estimate that $\sim 110 \text{ cm}$
326 of fine-grained matrix was removed from the top of the pediment by deflation (Fig. 9bB), resulting in a pavement of old
327 boulders at the top of a slowly eroding surface (Fig. 10), with minimum surface exposure ages between 0.569 and 1.377
328 My (Pleistocene). The Prince Albert area alluviated pediment has the youngest minimum exposure age of 0.569 My,
329 the Laingsburg area pediment has variable minimum exposure ages from 0.848 to 1.131 My. Over this timeframe, the
330 assumption of no erosion or deposition is an unlikely scenario. Assuming low erosion rates of 0.3 m My^{-1} (following
331 Bierman et al. 2014) the pediment minimum exposure ages increase substantially for the older surfaces, with minimum
332 ages ranging from 0.678 to 4.462 My (Table 3).

333
334 The ^{10}Be concentration depth profile provides more insights in the denudation process of the pediments. First, the uppermost
335 sample of the Laingsburg depth profile has a ^{10}Be concentration that is in line with the concentrations that are measured in

Formatted: Superscript

Formatted: Superscript

Formatted: Not Superscript/ Subscript

Formatted: Font: Not Bold, Font colour: Black, Border: : (No border)

Formatted: Not Highlight

Formatted: Superscript, Not Highlight

Formatted: Not Highlight

Formatted: Superscript

Formatted: Not Highlight

Formatted: Not Highlight

Formatted: Superscript

Formatted: Not Highlight

Formatted: Not Highlight

Formatted: Not Highlight

Formatted: Not Highlight

Formatted: Not Highlight

Formatted: Not Highlight

Formatted: Not Highlight

Formatted: Superscript, Not Highlight

Formatted: Not Highlight

Formatted: Not Highlight

Formatted: Not Highlight

Formatted: Not Highlight

Formatted: Not Highlight

Formatted: Not Highlight

Formatted: Not Highlight

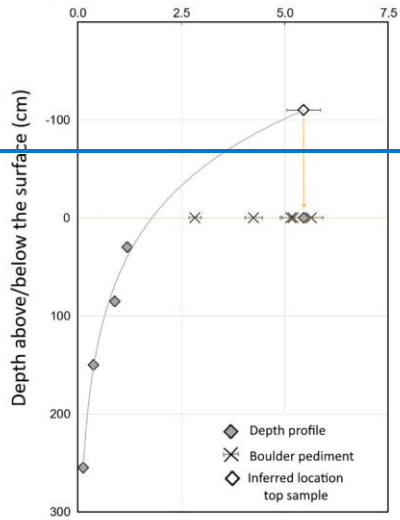
Formatted: Not Strikethrough

Formatted: Strikethrough

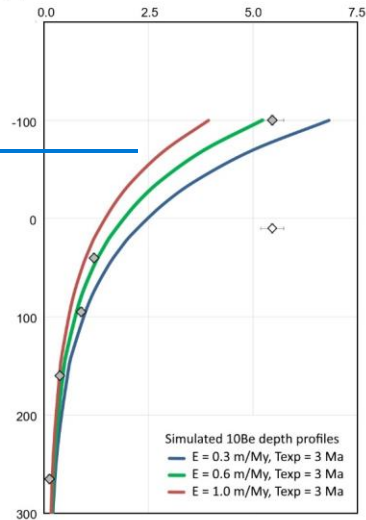
336 boulders sampled at the Laingsburg, Floriskraal and Leeuwgat alluviated pediments, and is markedly higher than the
337 concentration measured at the Prince Albert alluviated pediment (Fig. 9a, Table 3). Second, there is a large discrepancy in the
338 ^{40}Be concentrations between the uppermost sample and the four samples taken at depth in the profile (Table 2). The $4.265 \times$
339 10^6 at./g difference in ^{40}Be concentrations over a 30 cm depth increment cannot be explained by steady erosion of the pediment
340 after exposure (Fig. 9b). It suggests that deflation of ~110 cm of fine grained material at the surface of the pediments has
341 resulted in a pavement of old boulders at the top of a slowly eroding surface (Fig. 10).

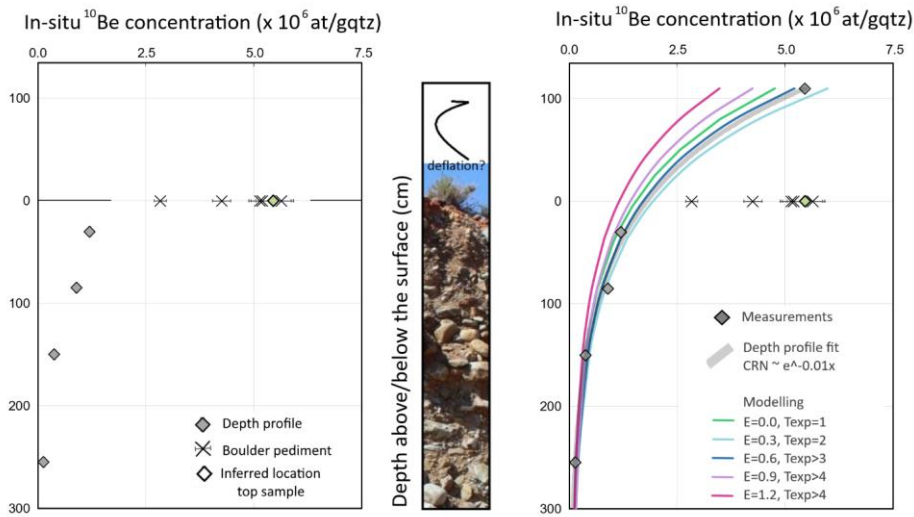
Formatted: Font colour: Black, Strikethrough, Border: : (No border)

(a) In-situ ^{10}Be concentration ($\times 10^6$ at/gqtz)



(b) In-situ ^{10}Be concentration ($\times 10^6$ at/gqtz)





343

344 **Figure 9: Depth profile results of the Laingsburg pediment. (a) showing in-situ ¹⁰Be concentrations (expressed in**
 345 **atoms of ¹⁰Be per g of quartz) as measured in depth profile and boulders from other pediments data listed in Table 3,**
 346 **and (b) modelled in-situ ¹⁰Be concentration from a data-fitted exponential model ($N_{10Be} \approx e^{-0.01 \times depth}$) and from**
 347 **numerical simulations using forward modelling for given erosion rates (E expressed in m My⁻¹) and exposure ages**
 348 **(T_{exp} expressed in Ma). For erosion rates exceeding 0.6 m My⁻¹, the in-situ ¹⁰Be concentrations are in secular**
 349 **equilibrium for exposure ages exceeding the T_{exp} indicated in the graph, and the concentration-depth profiles**
 350 **become time-invariant, showing erosion rate scenarios.**

351

352

Formatted: Superscript

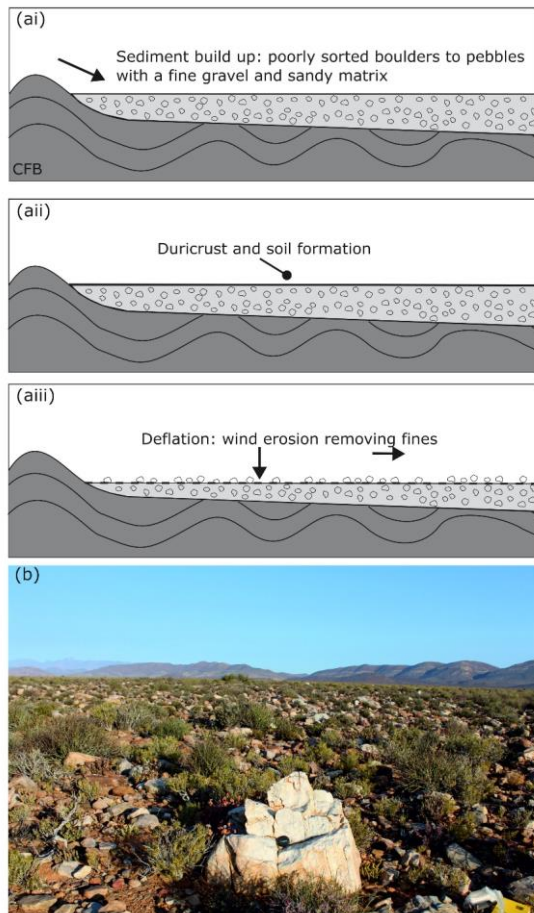
Formatted: Superscript

Formatted: Superscript

Formatted: Superscript

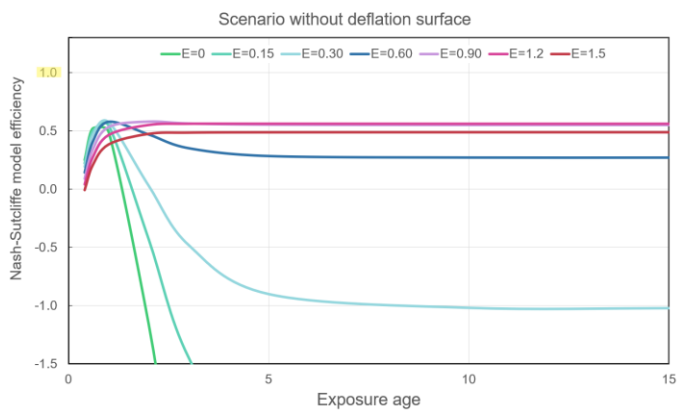
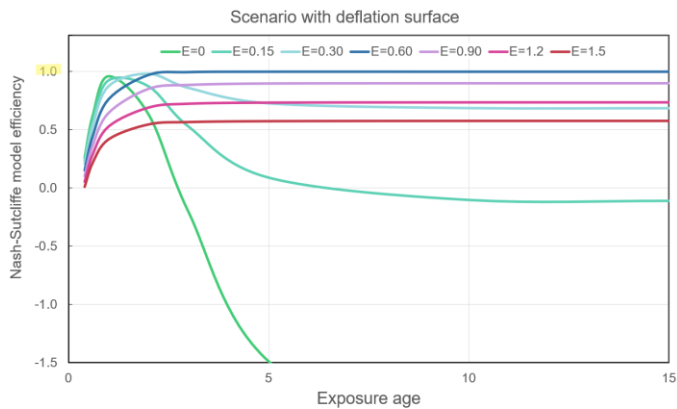
Formatted: Superscript

Formatted: Superscript



353

354 **Figure 100:** (a) Process of deflation and (b) Evidence of deflation: concentrations of boulders and pebbles on top of
 355 the Laingsburg Pediment.



356

357 **Figure 11:** Goodness-of-fit of the model predictions for the ^{10}Be depth concentration profile in the Laingsburg
 358 pediment, as evaluated by the Nash-Sutcliffe efficiency (NSE). The NSE ranges between $-\infty$ and 1, whereby 1
 359 corresponds to a perfect model fit. Model simulations were realised for a wide range of exposure ages (0 to 20 Ma)
 360 and denudation rates ($E = 0$ to 1.5 m My^{-1}), and for conditions with/without inheritance ($N_{inh}e^{-\lambda t} = N_{25500}$) and
 361 deflation ~~armor~~armouring. For simulations with development of armouring, optimal solutions ($\text{NSE} \rightarrow 1$) are found
 362 for denudation between 0.3 and 0.6 m My^{-1} and exposure ages exceeding 2 Ma . Model performances for simulations
 363 neglecting surface deflation are significantly lower ($\text{NSE} \rightarrow 0.6$), illustrating the necessity to account for deflation
 364 armouring.

365

- Formatted: Not Highlight
- Formatted: Superscript
- Formatted: Superscript
- Formatted: Not Highlight
- Formatted: Not Highlight
- Formatted: Not Highlight
- Formatted: Not Highlight
- Formatted: Not Highlight
- Formatted: Not Superscript/ Subscript, Not Highlight
- Formatted: Not Highlight
- Formatted: Not Superscript/ Subscript

366

367

368 [Based on Eq. 1, we modelled the ¹⁰Be concentration depth profile of the Laingsburg pediment for a wide spectrum of possible](#)
369 [erosion-exposure age scenarios. We evaluated the goodness-of-fit of the predicted models based on the Nash-Sutcliffe](#)
370 [efficiency \(NSE\) and chi-squared \(Fig. 11X\). Our results show no significant improvement in model performance when](#)
371 [accounting for inheritance, indicating that inheritance can be neglected in the analyses of the ¹⁰Be depth profiles in the](#)
372 [Laingsburg pediment. Otherwise, deflation of the surface is confirmed by the simulation outcomes because \(i\) model](#)
373 [predictions using erosion-exposure age scenarios that disregard deflation all have an NSE below 0.60 while their corresponding](#)
374 [scenarios accounting for deflation armoring have an NSE up to 1.00, and \(ii\) a two-sample comparison t-test confirms](#)
375 [significantly lower fit for model predictions that disregard deflation.](#)

376 [Optimal model fits, defined as model predictions with an NSE approaching ‘1’ and minimal chi-squared value, are obtained](#)
377 [for the scenarios with long-term erosion between 0.3 and 0.6 m My⁻¹, and exposure exceeding 2 Ma. Not only is this result](#)
378 [congruent with the outcomes of the CosmoCalc method \(Table 3\), it also provides more details on the erosion-exposure](#)
379 [scenarios that are most likely to explain the long-term evolution of the pediment.](#)

380 [When taking ablation of the upper ~110cm of the profile into account, the ¹⁰Be concentration depth profile of the Laingsburg](#)
381 [pediment can be simulated by forward modelling \(Vandermaelen et al., 2022\) using minimum age constraints from the surface](#)
382 [samples and information on the density of the overlying material from Kounov et al. \(2015\). The most likely denudation rate](#)
383 [of the pediment is ~0.6 m/My \(Figure 9b\), which is similar to the median erosion rate for South African pediment surfaces](#)
384 [reported by Bierman et al \(2014\). Even at this low surface lowering rate, the ¹⁰Be concentrations approach isotopic steady state](#)
385 [when the time of exposure exceeds 3 Ma, so that the age information derived from the depth profile only provides a *minimum*](#)
386 [exposure age.](#)

387 4.3 Elevations and grading of pediment

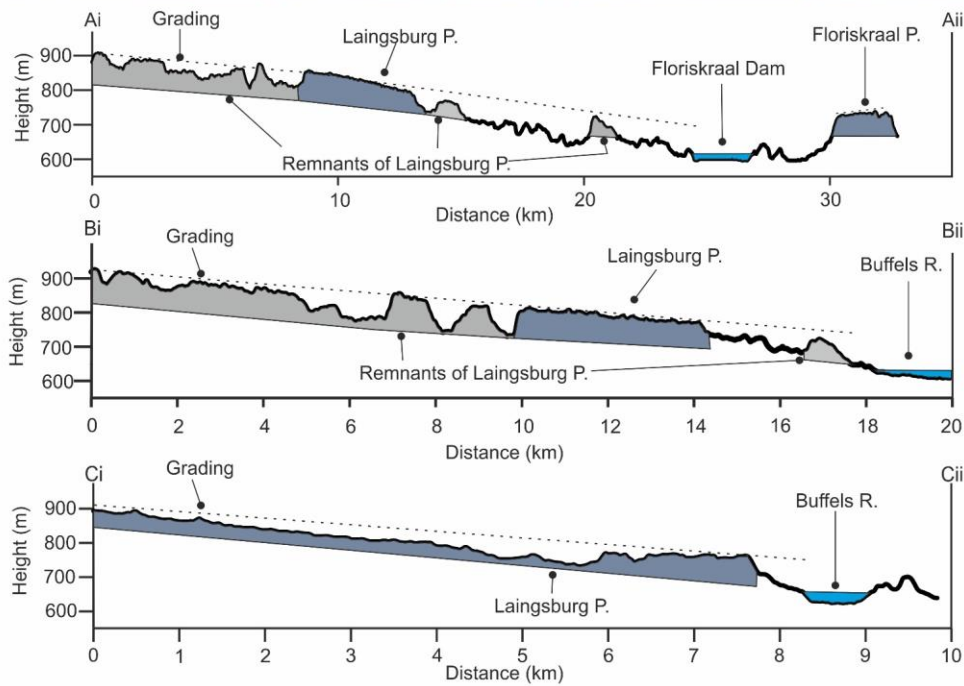
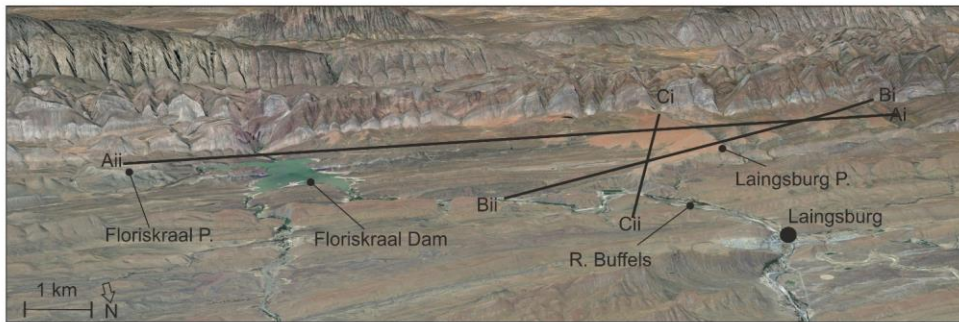
388 Figure 4c shows the pediment heights as classified by the Jenks natural break scheme (De Smith and Goodchild, 2007). The
389 alluviated pediments at Laingsburg and Floriskraal have elevations within the same class (714 – 870 m), and the Leeuwgat
390 and Prince Albert area alluviated pediments share the same elevation class (617 – 713 m). The Laingsburg area alluviated
391 pediment appears to have an aspect of slope that grades not only away from the CFB but towards the modern Buffels River
392 location, which abuts the northern limit of the alluviated pediment (Fig. 12f). This relationship is less clear on the Floriskraal
393 alluviated pediment, which is to the east of the Buffels River. The alluviated pediment at Leeuwgat, which sits between two
394 folds of the CFB, has no large trunk river nearby (~30 km from Dwyka River) and simply grades away from the CFB (Fig.
395 132aA). The Prince Albert area pediment grades towards the Gamka River, although it is currently ~16 km from the Gamka

Formatted: Not Highlight

Formatted: Superscript, Not Highlight

Formatted: Not Highlight

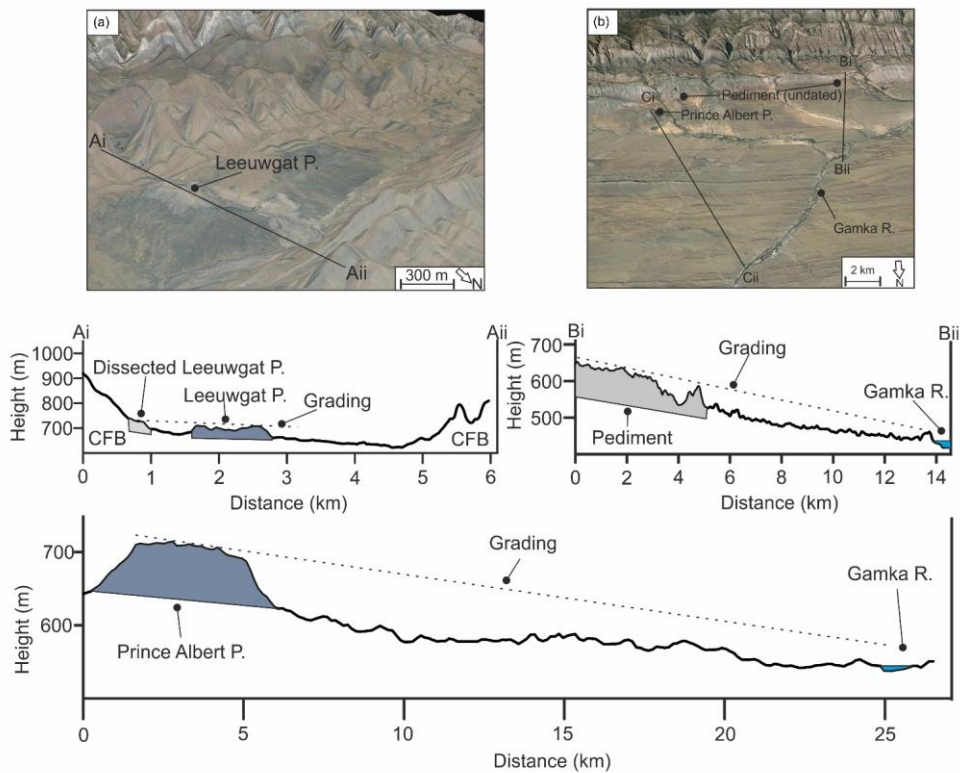
396 River (Fig. 132b). The fact that the alluviated pediments grade towards the present day trunk rivers but above their present day
 397 elevation indicates that these rivers were active during the formation of the pediments and is discussed later.
 398



399

400 **Figure 121:** Grading of the Laingsburg pediment and related cross sections, which grade not only away from the Cape
 401 Fold Belt but towards the Buffels River. Imagery from © Google Earth 2015.

402



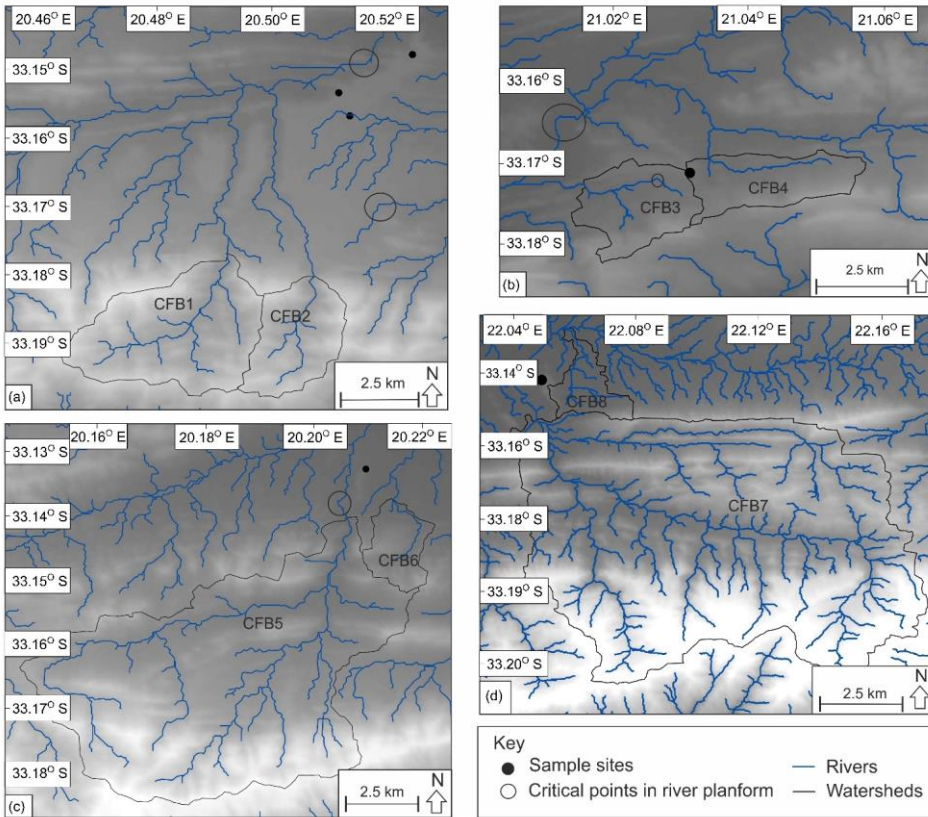
403 **Figure 132:** Grading of the (a) Leeuwgat, which grades away from the Cape Fold Belt and (b) Prince Albert pediment,
 404 which grades towards the Gamka River. Imagery (a) and (b) from © Google Earth 2015.

406

407 4.4. Dissecting river planform

408 The dissecting river planforms are shown in Fig. 143. critical-Critical points are highlighted that relate to sections where the
 409 rivers (i) have been deflected by the pediment surface, or (ii) have anomalous changes in orientation. Overall, the low order

410 rivers (<4) that have dissected the pediments are strongly influenced by the folding within the CFB (Richardson et al., 2016).
 411 This is especially seen within the rivers that have dissected the Laingsburg pediment (Fig. 143a), where the linear river
 412 planform aligns with the axis of a syncline. Where the rivers breach at the folds it appears that the presence of alluviated
 413 pediments deflected the river planforms; this relationship can also be seen at Floriskraal and Prince Albert area alluviated
 414 pediments (Fig. 143).



415

416 **Figure 143: Planforms of the dissecting rivers and Cape Fold Belt subcatchments; (a) Laingsburg; (b) Floriskraal; (c)**
 417 **Leeuwgat and; (d) Prince Albert. The circles highlight critical points related to deflection of the river planforms by the**
 418 **Cape Fold Belt or the pediment.**

419 4.5 Volume of material removed

420 Table 4 shows the bulk erosion rates related to dissection of the alluviated pediments post-post-formation. Converting this to
 421 an equivalent lithological thickness (dividing the volume of material removed over the area; Aguilar et al., 2011), an average
 422 of 141.43 m has been eroded around the large Laingsburg area pediment (Fig. 124). The Prince Albert area pediment, has an
 423 average lithological thickness of 42.33 m removed. Leeuwgat has had the least amount of dissection, with 17.25 m eroded.

424 **Table 4: Minimum volume of material eroded by rivers incising the pediment surface, the equivalent rock thickness**
 425 **and the time taken for incision using the average maximum denudation rate of 10.16 m My⁻¹ from Scharf et al., 2013**
 426 **and Kounov et al., 2015.**

Location	Volume of material removed (km ³)	Equivalent average rock thickness (m)	Time for incision (Ma)
Laingsburg	3.240	141.43	13.92
Floriskraal	0.154	42.33	4.17
Leeuwgat	0.169	44.27	4.36
Prince Albert	0.012	17.25	1.70

427

428 Table 5 shows the volume of material eroded by rivers draining the sub-catchments in the CFB, which have dissected the
 429 alluviated pediments. The sub-catchments range in area-size from 4.9 – 310 km², and the volume of material removed ranges
 430 from 0.11 - 89 km³, which is the equivalent of 21 - 286 m of lithological thickness. The alluviated pediments that are located
 431 further away from the CFB range have larger dissecting catchments associated with them. For example, the Laingsburg area
 432 alluviated pediment, which is backed by the CFB, has an average sub-catchment area of 14.37 km², whereas the Prince Albert
 433 area alluviated pediment is located ~ 2 km from the CFB and has an average sub-catchment area of 161.83 km². These sub-
 434 catchment areas are contributing to the incision of the pediments.

435

436

437

438

439

440

441 **Table 5: Minimum volume of material eroded by rivers draining the Cape Fold Belt sub-catchments, the equivalent**
 442 **rock thickness and the average time taken for incision using the average of the maximum denudation rate recorded**
 443 **from Scharf et al., 2013 and Kounov et al., 2015 of 10.16 m My⁻¹.**

Location	Catchment	Area (km ²)	Volume of material removed (km ³)	Equivalent average rock thickness (m)	Time for incision (Ma)
Laingsburg	CFB 1	19.79	2.86	144.39	14.21
	CFB 2	8.96	0.85	95.55	9.40
Floriskraal	CFB 3	6.21	0.28	45.31	4.46
	CFB 4	6.02	0.20	33.59	3.31
Leeuwgat	CFB 5	73.80	7.55	102.25	10.06
	CFB 6	4.91	0.11	21.64	2.13
Prince Albert	CFB 7	310.75	89.01	286.44	28.19
	CFB 8	12.92	0.23	17.79	1.75

444

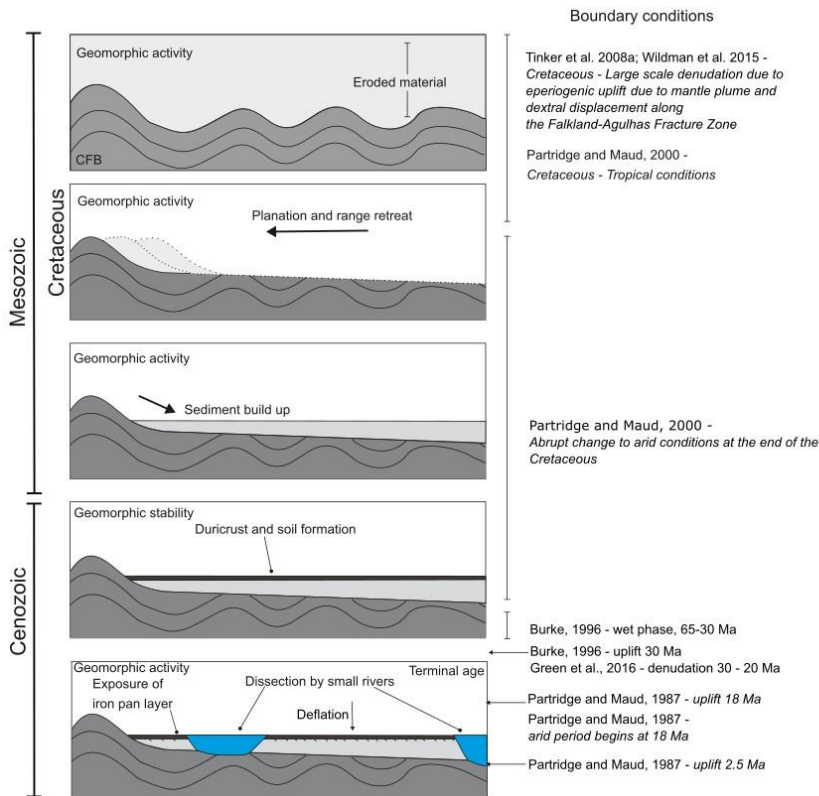
445 5. Discussion

446 5.1 Pediment formation and characteristics

447 The pediments are underlain by folded strata of the Karoo and Cape Supergroups (sandstone, siltstone and mudstone), and
 448 backed by the resistant CFB quartzites (Fig. 4b). It has been argued that pediments form on all lithology types, however the
 449 more extensive pediments can be found ~~above-on the least-less~~ resistant material (Dohrenward and Parsons, 2009). There is
 450 no systematic variation in pediment characteristics that can be related to the underlying geology (Fig. 4b).

451 The pediments have formed by diffusive processes, dominated by slope processes in the first stages of development, causing
 452 the gradual retreat of the Cape Fold Belt and coeval formation of colluvial material and ~~the~~ weathering mantle, including an
 453 iron pan (Fig. 154). There is no evidence of fluvial activity, such as clast imbrication, depositional or erosional bedforms, or
 454 channel-forms (Fig. 6; cf. e.g., Gilbert, 1877; Sharp, 1940; Lustig, 1969). The iron pan layer is now at the surface of the
 455 pediment due to the removal of overlying material as a result of surface deflation by wind erosion, as shown by the cosmogenic
 456 data from the ¹⁰Be concentration depth profile (Figs. 9, 154). The pediments grade towards, but above, large trunk rivers of
 457 the Gouritz catchment (Figs. 124, 132), indicating that large transverse systems were active before pediment planation and

458 colluvial build-up. The trunk rivers were also active during pediment formation, however they were probably less so, as shown
 459 by the build-up and preservation of material forming the pediments. This suggests that at the time of pediment formation there
 460 was deposition of colluvial material adjacent to large-scale sediment bypass via rivers, and formation of the pediment surfaces
 461 because of erosion processes. The trunk rivers, active during the formation of the pediments represent an upper limit to the
 462 extent of the pediments and the pediments should be regarded as individual landforms and not as an extensive regional 'surface'
 463 within the study area (cf. King, 1948, 1953, 1955; Partridge and Maud, 1987).



464

465 **Figure 154:** Sequence of events forming the pediments and boundary conditions; in which the folded Karoo
 466 Supergroup strata was planned, hillslope processes caused the build-up of sediment, soil formation and duricrust

467 **formation. The pediments were then dissected and fluvial processes dominate. In recent time, deflation processes**
468 **have dominated (Fig. 10).**

469 The distribution of the dissected pediments suggests that these are remnants of much more continuous local features (Fig. 132).
470 There has been a shift in the dominant process regime, from slope processes to fluvial processes, during the evolution of the
471 pediments as evidenced by the dissection of pediments by smaller rivers and the decoupling of the pediments from the CFB
472 sediment source area. The river planform has been primarily controlled by the orientation of tectonic folds. However, the
473 pediments could have also controlled the landscape evolution by deflecting the rivers, allowing the surfaces to be preserved.
474 It appears that the structural integrity of the pediment is not continuous across the entire pediment, ~~and areas.~~ Areas underlain
475 by cohesive material caused deflection of the dissecting rivers due to a higher resistance to erosion (Fig. 143). This could be a
476 function of the sedimentology (Fig. 6) of the pediment: the calibre of material; the extent of packing; or the presence and
477 thicknesses of the duricrust layer. Deflection of rivers has been shown to cause the formation of epigenetic gorges (Ouimet et
478 al., 2008). Furthermore, the pediments could have been preserved in these locations as rivers did not migrate laterally, which
479 could be due to variations in channel gradient. The pediments sit above the valley floor (current level of erosion) and are
480 fossilised landforms that represent a store of sediment that is mostly subject to slow denudation and weathering, followed by
481 and deflation under current climatic conditions (Fig. 10). ~~with hillslope processes~~ have slowly supplied ~~lying~~ sediment to
482 the nearby fluvial channels; however due to slow runoff rates related to the arid climate, the transport is no longer effective.
483

484 5.2 Implications of depth profile

485 ~~The ¹⁰Be CRN-concentration depth profile (Table 2 Fig. 9a) in the Laingsburg pediment indicates that the ¹⁰Be concentrations~~
486 ~~in the sedimentary sequence~~ deviate ~~s~~ from a simple exponential ~~concentration-concentration~~-depth profile. The stronger than
487 theoretically expected decrease in ¹⁰Be concentrations in the upper 30 cm ~~point-points~~ to a complex post-depositional history
488 of the alluviated pediment ~~at Laingsburg~~. The deviation can be explained by a ~~first-long~~ phase of low denudation rates (~~0.36~~
489 ~~to 0.6~~ m/My) followed by ~~a second phase of~~ aeolian deflation ~~of the surface~~ whereby finer material is preferentially removed.

490 Deflation has been reported for (semi-)arid environments during the Cenozoic (Binnie et al. 2020). The impact of deflation on
491 ¹⁰Be concentrations has been described for glacial outwash terraces (Hein et al. 2009; Darvill et al. 2015) where aeolian
492 deflation and bio- or cryoturbation caused previously buried cobbles to become exposed. It has also been recorded for
493 periglacial areas of central Europe where depth profiles ~~indicate-revealed~~ denudation rates of 40 to 80 m My⁻¹ during the
494 Quaternary (Ruszkiczay-Rudiger et al. 2011). Binnie et al. (2020) showed that deflation on marine terraces in Northern Chile
495 is the primary cause for multimodal distributions of ¹⁰Be concentration depth profiles.

496 Although the climate in southern South Africa has become more arid since the Cenozoic, the impact of aeolian deflation on
497 ¹⁰Be concentrations of pediment surfaces has not yet been addressed in previous work. Further work is needed to understand

Formatted: Font: 10 pt

Formatted: Font: 10 pt

498 if this behaviour is apparent across other pediment surfaces in the area, and how common this feature is across other pediment
499 surfaces.

Formatted: Font colour: Black, Border: : (No border)

500 The Our results also warrant for potential bias that can arise when from the ¹⁰Be concentration depth profile indicate that
501 caution should be taken when collecting only surface samples from alluvial pediment surfaces. ~~Boulders armouring/arming~~
502 the surface of alluvial pediments can be enriched in ¹⁰Be concentrations, compared to the sandy matrix, as they are residual
503 features. Their in-situ produced ¹⁰Be concentrations are pertinent to reconstructing exposure ages but underestimate surface
504 process rates. In contrast, sampling sand-sized material from the surface would have yield erroneous inferred ages that are too
505 young (Fig. 9b). There is an added value in sampling pediments at min. three depths covering a full path attenuation length, as
506 additional information on erosion-exposure age scenarios can be provided. Based on the complex ¹⁰Be concentration depth
507 profile in the Laingsburg pediment, CRN-based denudation rates from boulders could underestimate recent phases of surface
508 deflation. Further work is needed to understand if this behaviour is apparent across other pediment surfaces in the area, and
509 how common this feature is across other pediment surfaces. Future work should include concentration depth profiles from
510 other alluvial pediments to ascertain if surface deflation is occurring, and to account for this process when establishing regional
511 long-term denudation rates from CRN.

Formatted: Superscript

512 5.3 Geomorphic, tectonic, climatic and stratigraphic considerations

513 The cosmogenic data presented in Table 3 and Fig. 9 is within the range of data presented in Fig. 3 (van der Wateren and
514 Dunai, 2001; Bierman et al., 2014; Kounov et al., 2015). There is no systematic spatial variation in surface lowering rates of
515 the pediments that can be correlated to pediment size, or geology. The Prince Albert area alluviated pediment is the most
516 isolated from the CFB, with no duricrust present (Fig. 4a), which can explain why the surface lowering rates are the highest in
517 this location (0.954 m My⁻¹ compared to a maximum of 0.587 m My⁻¹ for the other pediments). Further, the pediment surfaces
518 only remain fossilised as long as the duricrust remains. When the duricrust is removed, denudation rates likely increase slightly
519 as shown by the Prince Albert area alluviated pediment, but will still remain low compared to other landforms (Fig. 3, Table
520 3). Therefore, the duricrusts represent an intrinsic geomorphic threshold. ~~By using forward modelling on the depth profile in~~
521 ~~the Laingsburg pediment, we demonstrated that the ¹⁰Be concentrations are at secular equilibrium, and that The ¹⁰Be derived~~
522 ~~exposure ages of the pediments are minimum estimates, and they reveal that the pediment has been exposed for more than 2~~
523 ~~My (Fig. 11). s are older than the Pleistocene, however, to further constrain this, geomorphic and stratigraphic information~~
524 ~~needs to be integrated.~~

Formatted: Superscript

Formatted: Not Highlight

525
526 The volume of material removed by river incision into the pediment surfaces equates to a lithological thickness of 42 to 141
527 m (Table 4). Assuming an average maximum denudation rate of the surrounding CFB area (10.16 m My⁻¹ from Scharf et al.,
528 2013 and Kounov et al., 2015), we can estimate that the dissection started as early as ~2 to 14 Ma ago. Cosmogenic and
529 thermochronological (apatite fission track and (U-Th)/He) studies have reported low denudation rates across the Cenozoic,

530 and Scharf et al. (2013) stated that the close agreement between the CRN-based denudation and AFTA/(U-Th)/He exhumation
531 rates is indicative of relative tectonic stability over the last 10^6 to 10^8 years.

532

533 As the dissection would have occurred after the formation of the alluviated pediments, they need to be older than the start of
534 the incision phase (2- 14 My). Based on the observed denudation of the sub-catchments within the CFB that back the pediments
535 and the mean maximum denudation rates from Scharf et al. 2013 and Kounov et al. 2015 (Figs. 3 and 8, Table 5), we obtain
536 indicative minimum ages of 9 - 14 My for the Laingsburg area pediment, 3 - 4 My for Floriskraal, 2 - 10 My for Leeuwgat and
537 2 – 28 My for Prince Albert. The CFB subcatchment denudation ages represent the ages of the dissecting rivers reaching the
538 CFB after dissecting the pediment surfaces. These indicative ages must be taken with caution as maximum published rates
539 have been used, and denudation rates vary over time, with a phase of increased erosion likely forming the incised channels.
540 ~~Nonetheless, the indicative ages are useful to put the *minimum* exposure ages from cosmogenic dating in context.~~ Furthermore,
541 as shown by the pediments causing the deflection of surrounding rivers (Fig. 143), denudation of the pediment material is slow
542 complicated (estimated between 0.3 and 0.6 m My⁻¹) further as the resistance of the pediment is higher than the surrounding
543 bedrock in some locations.

544

545 Using a combination of the data above, including data on the dissection of the pediment and backing subcatchments eroded
546 into the resistant Cape Fold Belt Catchments, the Laingsburg area pediment could have an age of 23 Ma; Floriskraal 8 Ma;
547 Leeuwgat 10 Ma; and Prince Albert 17 Ma. These age estimates correspond ~~to the to the timing of cessation of pediment~~
548 ~~formation and~~ start of dissection, and ~~are are~~ based on the assumption that geomorphic process rates were steady over long
549 timescales. The geomorphic evidence corroborates the outcomes of the numerical simulations of possible erosion-exposure
550 age scenarios for the Laingsburg pediment, uncovering the possibility of having very old (3 to > 15 My) exposed surfaces. As
551 denudation rates vary spatially and temporally, constant rates of erosion are unlikely as increased phases of activity are often
552 related to incision of the pediments. From geomorphic evidence, it is clear that the indicative ages are an order of magnitude
553 higher than the *minimum* exposure ages obtained from in situ produced cosmogenic nuclide concentrations. If the cosmogenic
554 *minimum* exposure ages are used, with the volume eroded recorded using the DEM, erosion rates range from 28 to 503 m Ma⁻¹
555 ¹ which further indicates the minimum exposure ages should be taken with caution as these extremely high erosion rates have
556 not been recorded using published studies (Fig. 3). Previous works have classified pediment surfaces within height brackets
557 (e.g., King, 1953). However, in this study there is no correlation between pediment elevation and their geomorphic ages.

558

559 Duricrusts are found in many of the studied alluviated pediments (Summerfield, 1983; Marker et al., 2002), and this is well-
560 developed in the Laingsburg area pediment (Fig. 5). The alluviated pediments no longer have the overlying weathering material
561 preserved, and have been lowered to the iron pan layer. The depth profile suggests that erosiondeflation has occurred after the
562 development of the weathering mantle (Fig. 9), which has exposed the iron pan (laterites). The iron pan could have formed by
563 leaching from surrounding lithologies and clasts, by lateral movement due to groundwater change (Widdowson, 2007), or by

Formatted: Superscript

564 deep weathering of the bedrock. Deep weathering with the formation of iron pans occurs on low relief surfaces that have been
565 stable for at least a million years (Al-Subary et al., 1998). Since the Cenozoic, South Africa has been relatively tectonically
566 quiescent (e.g., Bierman et al., 2014). In addition, a favourable climate of high annual rainfall, high humidity and high mean
567 annual temperature is required to form laterites (Widdowson, 2007). Further, higher concentrations of carbon dioxide are also
568 associated with the formation of laterites (and iron pans). Greenhouse episodes have occurred in the late Cretaceous and late
569 Palaeocene to early Eocene, leading to world-wide extensive weathering (Bardossy, 1981; Valetton, 1983).

570 Laterite development in southern South Africa is still poorly constrained. It has been argued to be late Pliocene in age (Marker
571 and Holmes, 1999) and have continued into the late Pleistocene (Marker and Holmes, 2005), being a component of the
572 Quaternary development of the Southern Cape (Marker et al., 2002). However, the Mediterranean climate (e.g., more humid)
573 of the coastal areas does not extend inland to the study location, which is expected for laterite development (Brown et al.,
574 1994; Braucher et al 1998a, b). Given the past climate and tectonic events, the iron pans probably formed during the late
575 Cretaceous greenhouse episode, which is compounded by the constrained dissection rates of the pediment surfaces (e.g.,
576 Dauteuil et al., 2015). The formation of duricrusts and iron pans would have occurred coevally with pediment formation, and
577 would have extended post-pediment formation (Helgren and Butzer, 1977; Widdowson, 2007). The presence of iron pans
578 indicates a period of geomorphic stability ~~that can have lasted more than 2 My with low (0.3 to 0.6 m My⁻¹) denudation rates,~~
579 ~~within the development of the landforms of at least 1 Ma, and probably much longer and could have occurred during the~~
580 ~~denudation of the pediments.~~

Formatted: Superscript

581 5.4 Sequence of events

582 Pediment formation requires mountain range retreat, which causes the underlying lithological strata to be truncated (Fig. ~~ure~~
583 154). The *minimum* exposure ages calculated by cosmogenic nuclide dating using the boulder surface samples show
584 remarkably low denudation rates of the pediments during the last 3.8 Myr, which is related both to lithology (duricrust
585 cappings, resistant quartzite boulders; e.g., Scharf et al., 2013) and structure of the CFB deflecting incising rivers. ~~The complex~~
586 ~~concentration depth profile indicates that a recent phase of deflation has occurred, as there exists a discrepancy between the~~
587 ~~CRN concentration of the residual boulders at the surface, and the boulders that are embedded in a sandy matrix at 30 cm~~
588 ~~depth. It is important to integrate geomorphologic and stratigraphic knowledge when reporting cosmogenic nuclide results,~~
589 ~~especially in an ancient setting with low denudation rates where the nuclide concentrations may reach secular equilibrium to~~
590 ~~further extend the landscape development history.~~

591 During the Cretaceous the Cape Fold Belt was exhumed (Fig. 154; Tinker et al. 2008a, Tankard et al. 2009). During this time,
592 the folded strata was eroded and planed by hillslope processes (e.g., Rich, 1935; Bourne and Twidale, 1998), depositing
593 colluvial material and then forming soils (Fig. 154) on the alluviated pediments. This was aided by the humid climate and
594 greenhouse conditions of the Cretaceous causing deep weathering (Bardossy, 1981; Valetton, 1983). Tectonic stability allowed
595 the formation of iron pans and duricrusts, which are now exposed at the surface of the alluviated pediments due to surface

596 deflation and the removal of overbank material, as shown by the depth profile (Fig. 154). The initial planation and colluvial
597 build-up had to have occurred pre-Miocene as shown by the dissection data (Tables 4, 5). However, we posit the surfaces could
598 have formed much earlier due to the very slow processes associated with pediment formation (e.g., Lustig, 1969; Dohrenwend
599 and Parsons, 2009). By the mid-Miocene, dissection of the pediments and backing Cape Fold Belt occurred with the
600 development of small streams and subcatchments draining the pediments, with a shift towards a more fluvial dominated regime.
601 This latter stage of landscape development has decoupled the pediments from the CFB sediment source, and essentially
602 fossilised the landform (Table 3), with very low ~~surface-loweringdenudation~~ (0.3 to ~0.6 m⁴My⁻¹) ~~followed by and~~ a more
603 recent phase of aeolian deflation.

Formatted: Superscript

604 5.5 Implications for landscape development

605 The evolution of the pediment surfaces studied in South Africa ~~indicate-indicates~~ that the relative importance of hillslope and
606 fluvial processes (including valley development) varies over time. Therefore, the model proposed here does not fit into the
607 previously published model types (Fig. 1) that argued ~~that~~ pediment evolution is dominated by a single process (e.g., 'Model
608 1' Figure 1; Gilbert, 1877; Paige, 1912; Howard 1942 and 'Model 2' Fig. 1; Lawson, 1915; Rich; 1935; Kesel, 1977; Bourne
609 and Twidale, 1998; Dauteuil et al., 2015), ~~that the dominant processee~~ varies due to lithology (e.g., 'Model 3' Figure 1: Lustig,
610 1969; Parsons and Abrahams, 1984) or is assisted by ~~valley-/basinvalley/basin~~ development (e.g., 'Model 4' Fig. 1; Lustig,
611 1969; Parsons and Abrahams, 1984). The change from hillslope to fluvial processes is likely a response to tectonic or climatic
612 perturbations (Fig. 154). The initial formation of the pediments was most likely aided by large-scale erosion during the
613 Cretaceous (e.g., Tinker et al., 2008a,b; Wildman et al., 2015, 2016; Richardson et al., 2017) and tropical ~~climate~~ conditions
614 (Partridge and Maud, 2000).

615 The indicative geomorphic ages reported here, related to the second phase of development and the dissection of the pediments
616 by small tributaries, roughly correlate to the proposed uplift in the Cenozoic (Green et al., 2016) of 30 Ma (Burke, 1996), 18
617 Ma (Partridge and Maud, 1987) and 2.5 Ma (Partridge and Maud, 1987), and could indicate that the pediments were dissected
618 due to different pulses of uplift. Nonetheless, this time period also corresponds to variation in climate, including periods of
619 humidity reported to have ended at 30 Ma (Burke, 1996) or 18 Ma (Burke, 1996). It is not possible to distinguish the main
620 driver of dissection, and tectonic signatures are not identified within the Gouritz catchment morphometry (Richardson et al.,
621 2016).

622 The grading of the pediments ~~indicates-implies that~~ the main trunk rivers were active before the ~~development of the~~ pediments,
623 at least by the Miocene and probably ~~established~~ within the Cretaceous; when large scale exhumation occurred within South
624 Africa (e.g., Tinker et al. 2008a, Richardson et al., 2017). The individual grading of the pediment surfaces indicates the
625 pediments are relatively local features that react to surrounding tectonic, geological, and geomorphological settings, and are
626 not singular surfaces (King, 1953). ~~The ¹⁰Be-derived denudation rates of the pediments are some of the lowest in the world~~
627 ~~(Portenga and Bierman, 2011), and congruent with The surface-lowering-rates-of-the-pediments-indicate-a-period-of-low~~

Formatted: Superscript

628 geomorphic activity as documented by other researchers (Fig. 3, and references therein). There has been a drastic reduction in
629 denudation rates since the Cretaceous as shown by apatite fission track and cosmogenic nuclide studies (Fig. 3 and references
630 therein). ~~The data reported in this study are some of the lowest in the world (Portenga and Bierman, 2011). However,~~ Surface
631 lowering is not consistent across landforms within southern South Africa. Rivers are dissecting at a faster rate (Scharf et al.,
632 2013; Kounov et al., 2015) than the pediment surfaces (this study, van der Water~~an~~ and Dunai, 2001; Bierman et al., 2014;
633 Kounov et al., 2015), which indicates that relief is developing at a slow rate, as also reported by Bierman et al. (2014) from
634 the Eastern Cape. The offshore depositional record (Tinker et al. 2008a) mirrors the reduction in denudation rates with peaks
635 in the Cenozoic most likely related to the rejuvenation of the landscape, which dissected the pediments in this study (e.g.,
636 Hirsch et al., 2010; Dalton et al., 2015; Sonibare et al., 2015). These increases in offshore sediment flux are minor in
637 comparison to rates in the Cretaceous.

638 6. Conclusion

639 Large-scale erosional surfaces characterise the ancient landscape of southern South Africa. Denudation rates of the Prince
640 Albert and Laingsburg pediments in the Western Cape are between 0.3 and 1.0 m My⁻¹, and the pediments have been exposed
641 before. Cosmogenic nuclide dating using ¹⁰Be of four pediment surfaces in the Western Cape, and a depth profile indicate low
642 surface lowering rates (0.315 to 0.954 m My⁻¹) and minimum exposure ages from the Early Pleistocene. As most of the
643 pediment surfaces have ¹⁰Be concentrations that approach secular equilibrium, the ¹⁰Be-derived Given that the isotope
644 concentrations are close to isotopic steady state, the ¹⁰Be-derived exposure ages are minimum provide minimum exposure age
645 e estimates. Our study corroborates how CRN depth Cosmogenic radionuclide depth profiling profiling in alluvial pediments
646 can provide additional information on long-term landscape dynamics, and demonstrates how forward modelling can unveil the
647 erosion-exposure age scenarios that most likely explain the observed ¹⁰Be depth concentrations. The existence of a long period
648 of low denudation followed by a recent phase of aeolian revealed that the post-depositional history of the alluviated pediments
649 is likely to be complex, with a long period of slow denudation that is followed by a phase of aeolian deflation merits further
650 study. Further work, beyond the scope of this study is needed, to understand verify if this is a widespread and characteristic
651 feature of alluviated pediment surfaces in (semi-)arid climatic conditions.

652 The pediments studied must be at least Miocene in age, and probably much older (i.e. Cretaceous) based on the volumes of
653 post-pediment dissection, published erosion rates, the presence of duricrusts and the current understanding of tectonic and
654 climatic variation in the region. The duricrusts represent an internal geomorphic threshold which limits the rate of denudation.
655 The dissection of the pediments has been largely controlled by the structure of the Cape Fold Belt, with the initial geomorphic
656 pulse of incision most likely related to tectonic uplift or climate change. The pediments grade to individual base levels (trunk
657 rivers), and although locally extensive, they are not a regional feature representing one single surface. The presence of the
658 pediments deflected dissecting rivers in some locations and controlled landscape evolution of the surrounding rivers.

Formatted: Superscript

Formatted: Superscript

659 The pediments in southern South Africa are lowering at very low rates and are now decoupled from the surrounding rivers.
660 Therefore, they are a fossilised landform that represents a relatively stable store of sediment in which surface lowering occurs
661 by aeolian erosion causing deflation. The persistence of the pediments is due to the resistant duricrust capping and quartzitic
662 boulders, and the structural control of the Cape Fold Belt and pediments, deflecting dissecting rivers. We contend that [a multi-
663 proxy approach that combines cosmogenic nuclides results must not be viewed in isolation and should be assessed together
664 with surrounding geomorphologic and stratigraphic conditions provides a more comprehensive picture of long-term
665 landscape dynamics.](#)

666

667 **Supplement**

668 **Cosmogenic data used in this study is provided as a supplement.**

Formatted: Heading 1, Left, Line spacing: single

Formatted: Font: Bold

669 **Author Contributions**

670 Janet C. Richardson, David Hodgson and Andreas Lang collected the data. Processing and analysis of the data was completed
671 by Janet C. Richardson and Veerle Vanacker. [Forward modelling work was completed by Veerle Vanacker.](#) Marcus Christl
672 measured the $^{10}\text{Be}/^9\text{Be}$ using an accelerator mass spectrometer on the 500 kV Tandy facility at ETH Zürich. Veerle Vanacker
673 provided further support processing the data with regards to the depth profile, creating Figure 9 and writing the methodology
674 for cosmogenic nuclides. Janet C. Richardson led the writing and drafting of figures, with contributions on the text and figures
675 by Veerle Vanacker, David Hodgson and Andreas Lang.

676 **Acknowledgements**

677 The British Geomorphology Society (BSG) and British Sedimentology Research Group (BSRG) are thanked for providing
678 postgraduate grants to J. Richardson for completing this research. Jérôme Schoonejans and Marco Bravin are thanked for their
679 help during laboratory work undertaken in Université catholique de Louvain, Belgium. David Lee is thanked for his help in
680 improving Fig. 1. The landowners in South Africa are thanked for their permission to enter their land and take samples. The
681 Council of Geoscience are thanked for providing Geology GIS tiles, under the Academic/Research license. Alexandre Kounov
682 and an anonymous reviewer are thanked for their reviews of a previous version of this paper.

683

684 **Competing interests**

685 Andreas Lang is a member of the editorial board for Earth Surface Dynamics.

686 **References**

- 687 Abdelkareem, M., Ghoneim, E., El-Baz, F., and Askalany, M.: New insight on paleoriver development in the Nile basin of the
688 eastern Sahara. *J. of Afr. Ear. Sci.*, 62, 35-40, doi: 10.1016/j.jafrearsci.2011.09.001, 2012.
- 689 Aguilar, G., Riquelme, R., Martinod, J., Darrozes, J. and Maire, E.: Variability in erosion rates related to the state of landscape
690 transience in the semi-arid Chilean Andes. *ESPL*, 36, 1736-1748, doi: 10.1002/esp.2194, 2011.
- 691 Al-Subbary, A.K., Nichols, G.J., Bosence, D.W.J. and Al-Kadasi, M.: Pre-rift doming, peneplanation or subsidence in the
692 southern Red Sea? Evidence from the Medj-Zir Formation (Tawilah Group) of western Yemen. In: Purser BH, Bosence D.
693 (eds.) *Sedimentation and Tectonics in Rift Basins Red Sea:-Gulf of Aden*. Springer Netherlands. pp. 119-134, 1998
- 694 Balco, G., Stone, J.O., Lifton, N.A. and Dunai, T.J.: A complete and easily accessible means of calculating surface exposure
695 ages or erosion rates from 10 Be and 26 Al measurements. *Q. Geochron.*, 3: 174-195, doi: 10.1016/j.quageo.2007.12.001,
696 2008.
- 697 Bardossy, G.: Paleoenvironments of laterites and lateritic bauxites – effect of global tectonism on bauxite formation. In:
698 *International Seminar on Lateritisation Processes (Trivandrum, India)*. Rotterdam: Balkema, pp. 284–297, 1981
- 699 Bellin N, Vanacker V, Kubik PW. Denudation rates and tectonic geomorphology of the Spanish Betic Cordillera. *EPSL*, 390:
700 19-30, doi: 10.1016/j.epsl.2013.12.045, 2014.
- 701 Bessin, P., Guillocheau, F., Robin, C., Schrötter, J.M., Bauer, H.: Planation surfaces of the Armorican Massif (western France):
702 Denudation chronology of a Mesozoic land surface twice exhumed in response to relative crustal movements between Iberia
703 and Eurasia. *Geomorph.*, 233: 75-91, doi: 10.1016/j.geomorph.2014.09.026, 2015.
- 704 Bierman, P.R. and Caffee, M.: Slow rates of rock surface erosion and sediment production across the Namib Desert and
705 escarpment, southern Africa. *Am. J. Sci.*, 301, 326-358, 2001.
- 706 Bierman, P.R., Coppersmith, R., Hanson, K., Neveling, J., Portenga, E.W. and Rood, D.H.: A cosmogenic view of erosion,
707 relief generation, and the age of faulting in southern Africa. *GSA Today*, 24: 4-11, doi: 10.1130/GSATG206A.1, 2014.
- 708 Binnie, A., Binnie, S.A., Parteli, E.J.R. and Dunai, T.J.: The implications of sampling approach and geomorphological
709 processes for cosmogenic 10Be exposure dating of marine terraces. *Nucl. Instrum. and Methods Phys. Res. Sec. B*, 467, 130-
710 139, doi: 10.1016/j.nimb.2019.12.017, 2020.
- 711 Bishop, P.: Long-term landscape evolution: linking tectonics and surface processes. *ESPL*, 32: 329-365, doi:
712 10.1002/esp.1493, 2007.
- 713 Bloom, A.L.: Teaching about relict, no-analog landscapes. *Geomorph.*, 47: 303-311, doi: 10.1016/S0169-555X(02)00094-6 ,
714 2002.
- 715 Bourne, J.A. and Twidale, C.R.: Pediments and alluvial fans: genesis and relationships in the western piedmot of the Flinders
716 Ranges, South Australia. *Aust. J. Earth Sci.*, 45: 123–135, doi: 10.1080/08120099808728373, 1998.
- 717 Braucher, R., Bourles, D.L., Colin, F., Brown, E.T. and Boulange, B.: Brazilian laterite dynamics using in situ-produced 10
718 Be. *EPSL*, 163: 197-205, doi: 10.1016/S0012-821X(98)00187-3, 1998.

719 Braucher R., Colin, F., Brown, E.T., Bourles, D.L., Bamba, O., Raisbeck, G.M., You, F. and Koud, J.M.: African laterite
720 dynamics using in situ-produced 10 Be. *Geochem. Cosmo. Acta*, 62, 1501-1507, doi: 10.1016/S0016-7037(98)00085-4, 1998.

721 Braucher, R., Brown, E.T., Bourlès, D.L. and Colin, F.: In situ produced 10 Be measurements at great depths: implications for
722 production rates by fast muons. *EPSL*, 211, 251-258, doi: 10.1016/S0012-821X(03)00205-X, 2003.

723 Braucher, R., Merchel, S., Borgomano, J. and Bourlès, D.L.: Production of cosmogenic radionuclides at great depth: A
724 multielement approach, *EPSL*, 309, 1–9, doi: 10.1016/j.epsl.2011.06.036 , 2011.

725 Braun, J., Guillocheau, F., Robin, C., Baby, G. and Jelsma, H.: Rapid erosion of the Southern African Plateau as it climbs over
726 a mantle superswell. *J. Geophys. Res.: Solid Earth*: 119, 6093-6112, doi: 10.1002/2014JB010998, 2014.

727 Brocklehurst, S.H. and Whipple, K.X.: Glacial erosion and relief production in the Eastern Sierra Nevada, California.
728 *Geomorph.*, 42, 1–24, doi: 10.1016/S0169-555X(01)00069-1, 2002.

729 Brook, E.J., Brown, E.T., Kurz, M.D., Ackert, R.P., Raisbeck, G.M. and Yiou, F.: Constraints on age, erosion, and uplift of
730 Neogene glacial deposits in the Transantarctic Mountains determined from in situ cosmogenic 10Be and 26Al. *Geol.*, 23, 1063-
731 1066, doi: 10.1130/0091-7613(1995)023<1063:COAEAU>2.3.CO;2, 1995.

732 Brown, E.T., Bourlès, D.L., Colin, F., Sanfo, Z., Raisbeck, G.M., and Yiou, F.: The development of iron crust lateritic systems
733 in Burkina Faso, West Africa examined with in-situ-produced cosmogenic nuclides. *EPSL*, 124, 19-33, doi: 10.1016/0012-
734 821X(94)00087-5, 1994.

735 Brown, R.W., Rust, D.J., Summerfield, M.A., Gleadow, A.J. and De Wit, M.C.: An Early Cretaceous phase of accelerated
736 erosion on the south-western margin of Africa: Evidence from apatite fission track analysis and the offshore sedimentary
737 record. *Int. J. Rad. Appl. Instr. A. Part D. Nucl. Tracks and Radiat. Meas.*, 17, 339-350, doi: 10.1016/1359-0189(90)90056-
738 4, 1990.

739 Brown, R.W., Summerfield, M.A. and Gleadow, A.J.W.: Denudation history along a transect across the Drakensberg
740 Escarpment of southern Africa derived from apatite fission track thermochronology. *J. Geophys. Res.*, 107, 1-18, doi:
741 10.1029/2001JB000744, 2002.

742 Bryan, K.: Erosion and sedimentation in the Papago country, Arizona. *U.S. Geol. Surv. Bull.*, 730, 19–90, 1923.

743 Burbank, D.W., Leland, J., Fielding, E., Anderson, R.S., Brozovic, N., Reid, M.R. and Duncan, C.: Bedrock incision, rock
744 uplift and threshold hillslopes in the northwestern Himalayas. *Nature*, 379, 505-510, 1996.

745 Burke, K. The African plate. *S. Afri. J. Geol.*, 99, 341-409, 1996.

746 Carignano, C., Cioccale, M., and Rabassa, J.: Landscape antiquity of the Central Eastern Sierras Pampeanas (Argentina):
747 Geomorphological evolution since Gondwanic times. *Z. Geomorph. Supplement Band 118*, 245–268, 1999.

748 Chadwick, O.A., Roering, J.J., Heimsath, A.M., Levick, S.R., Asner, G.P. and Khomo, L.: Shaping post-orogenic landscapes
749 by climate and chemical weathering. *Geol.*, 41, 1171-1174, doi: 10.1130/G34721.1, 2013.

750 Chappell, J., Zheng, H. and Fifield, K.: Yangtse River sediments and erosion rates from source to sink traced with cosmogenic
751 10 Be: Sediments from major rivers. *Palaeo.*, 241, 79-94, doi: 10.1016/j.palaeo.2006.06.010, 2006.

752 Chmeleff, J., von Blanckenburg, F., Kossert, K. and Jakob, D.: Determination of the ^{10}Be half-life by multicollector ICP-MS
753 and liquid scintillation counting. *Nucl. Instrum. and Methods in Phys. Res. B*, 263, 192–199, doi: 10.1016/j.nimb.2009.09.012,
754 2010.

755 Chorley, R.J., Schumm, S.A. and Sugden, D.E.: *Geomorphology*, London. Methuen and Co. 648 pp, 1984.

756 Christl, M., Vockenhuber, C., Kubik, P.W., Wacker, L., Lachner, J., Alfimov, V. and Sinal, H-A.: The ETH Zurich AMS
757 facilities: Performance parameters and reference materials. *Nucl. Instrum. and Methods in Phys. Res. B*, 294, 29-38, doi:
758 10.1016/j.nimb.2012.03.004, 2-13, 2013.

759 Cockburn, H.A.P., Brown, R.W., Summerfield, M.A. and Seidl, M.A.: Quantifying passive margin denudation and landscape
760 development using a combined fission-track thermochronology and cosmogenic isotope analysis approach. *EPSL*, 179, 429-
761 435, doi: 10.1016/S0012-821X(00)00144-8, 2000.

762 Codilean, A.T., Bishop, P., Stuart, F.M., Hoey, T.B., Fabel, D. and Freeman, S.P.: Single-grain cosmogenic ^{21}Ne
763 concentrations in fluvial sediments reveal spatially variable erosion rates. *Geol.*, 36, 159-162, doi: 10.1130/G24360A.1, 2008.

764 Dalton, T.J.S., Paton, D.A., Needham, T. and Hodgson, N.: Temporal and spatial evolution of deepwater fold thrust belts:
765 Implications for quantifying strain imbalance. *Interpret.*, 3, SAA59-SAA70, doi: 10.1190/INT-2015-0034.1, 2015.

766 Darvill, C.M., Bentley, M.J., Stokes, C.R., Hein, A.S. and Rodés, Á.: Extensive MIS 3 glaciation in southernmost Patagonia
767 revealed by cosmogenic nuclide dating of outwash sediments. *EPSL*, 429, 157-169, doi: 10.1016/j.epsl.2015.07.030, 2015.

768 Dauteuil, O., Bessin, P. and Guillocheau, F.: Topographic growth around the Orange River valley, southern Africa: A Cenozoic
769 record of crustal deformation and climatic change. *Geomorph.*, 233, 5-19, doi: 10.1016/j.geomorph.2014.11.017, 2015.

770 Davis, W.M. *Observations in South Africa*. *Geol. Soc. Am. Bull.*, 17, 377-450, 1906.

771 Dean, W.R.J., Hoffinan, M.T., Meadows, M.E. and Milton, S.J.: Desertification in the semi-arid Karoo, South Africa: review
772 and reassessment. *J. Arid Env.*, 30, 247-264, doi: 10.1016/S0140-1963(05)80001-1, 1995.

773 Decker, J.E., Niedermann, S. and de Wit, M.J.: Soil erosion rates in South Africa compared with cosmogenic ^3He -based rates
774 of soil production. *S. Afri. J. Geol.*, 114, 475-488, doi: 10.2113/gssajg.114.3-4.475, 2011.

775 Decker, J.E., Niedermann S. and de Wit, M.J.: Climatically influenced denudation rates of the southern African plateau: Clues
776 to solving a geomorphic paradox. *Geomorph.*, 190, 48-60, doi: 10.1016/j.geomorph.2013.02.007, 2013.

777 Doucouré, C.M. and de Wit, M.J.: Old inherited origin for the present near-bimodal topography of Africa. *J. Afr. Earth Sci.*,
778 36, 371-388, doi: doi.org/10.1016/S0899-5362(03)00019-8, 2003

779 Demoulin, A., Zárata, M. and Rabassa, J.: Long-term landscape development: a perspective from the southern Buenos Aires
780 ranges of east central Argentina. *J. S Am. Earth Sci.*, 19, 193–204, doi: 10.1016/j.jsames.2004.12.001, 2005.

781 De Smith, M.J., Goodchild, M.F. and Longley, P.: *Geospatial analysis: a comprehensive guide to principles, techniques and*
782 *software tools*. Troubador Publishing Ltd. pp. 389, 2007.

783 de Wit M.: The Kalahari Epeirogeny and climate change: differentiating cause and effect from core to space. *S. Afri. J. Geol.*,
784 110, 367-392, doi: 10.2113/gssajg.110.2-3.367, 2007.

785 Dirks, P.H., Kibii, J.M., Kuhn, B.F., Steininger, C., Churchill, S.E., Kramers, J.D., Pickering, R., Farber, D.L., Mériaux, A.S.,
786 Herries, A.I. and King G.C. Geological setting and age of Australopithecus sediba from southern Africa. *Sci*, 328, 205-208,
787 doi: 10.1126/science.1184950, 2010.

788 Dixey, F.: African landscape. *Geograph. Rev.*, 34, 457-465, doi: 10.2307/209976, 1944.

789 Dohrenwend, J.C. and Parsons, A.J.: Pediments in arid environments. In: Abrahams, A.D., Parsons, A.J. (Eds.)
790 *Geomorphology of desert environments*. Springer Netherlands. pp. 377-411, 2009.

791 Doucouré CM, de Wit MJ. 2003. Old inherited origin for the present near bimodal topography of Africa. *J. Afri. Earth Sci.*,
792 36, 371-388, doi: 10.1016/S0899-5362(03)00019-8, 2003.

793 Dunai, T.J.: Scaling factors for production rates of in situ produced cosmogenic nuclides: a critical reevaluation, *EPSL*, 176,
794 157-169, doi: 10.1016/S0012-821X(99)00310-6, 2000.

795 Dunai TJ. 2010. *Cosmogenic Nuclides: Principles, Concepts and Applications in the Earth Surface Sciences*, Cambridge
796 University Press, Cambridge, UK, 2010.

797 Dunai, T.J., López, G.A.G. and Juez-Larré, J.: Oligocene-Miocene age of aridity in the Atacama Desert revealed by exposure
798 dating of erosion-sensitive landforms. *Geol.*, 33, 321-324, doi: 10.1130/G21184.1, 2005.

799 Du Toit, A.: *Our Wandering Continents*. Oliver and Boyd, U.K, 366 pp, 1937.

800 Du Toit, A.: *The Geology of South Africa*, 3rd edn. Oliver and Boyd, U.K. 539 pp, 1954.

801 Ebinger, C.J. and Sleep, N.H.: Cenozoic magmatism throughout east Africa resulting from impact of a single plume. *Nature*,
802 395, 788-791, 1998.

803 Erlanger, E.D., Granger, D.E. and Gibbon, R.J.: Rock uplift rates in South Africa from isochron burial dating of fluvial and
804 marine terraces. *Geol.*, 40, 1019-1022, doi: 10.1130/G33172.1, 2012.

805 Fleming, A., Summerfield, M.A., Stone, J.O., Fifield, L.K. and Cresswell, R.G.: Denudation rates for the southern Drakensberg
806 escarpment, SE Africa, derived from in-situ-produced cosmogenic ³⁶Cl: initial results. *J. Geol. Soc.*, 156, 209-212, doi:
807 10.1144/gsjgs.156.2.0209, 1999.

808 Flowers, R.M. and Schoene, B.: (U-Th)/He thermochronometry constraints on unroofing of the eastern Kaapvaal craton and
809 significance for uplift of the southern African Plateau. *Geol.*, 38, 827-830, doi: doi.org/10.1130/G30980.1, 2010.

810 [Frimmel, H.E., Fölling, P.G. and Diamond, R.: Metamorphism of the Permo-Triassic Cape Fold Belt and its basement, South](#)
811 [Africa. *Min. and Pet.*, 73, 325-346, 2001.](#)

812 Gallagher, K. and Brown, R.: The Mesozoic denudation history of the Atlantic margins of southern Africa and southeast Brazil
813 and the relationship to offshore sedimentation. *Geol. Soc., London, Sp. Pub.*, 153, 41-53, doi: 10.1144/GSL.SP.1999.153.01.0,
814 1999.

815 Ghosh, P., Sinha, S. and Misra, A.: Morphometric properties of the trans-Himalayan river catchments: Clues towards a relative
816 chronology of orogen-wide drainage integration. *Geomorph.*, 233, 127-141, doi: 10.1016/j.geomorph.2014.10.035, 2014.

817 Gilbert, G.K.: Report on the geology of the Henry Mountains. US Geographical and Geological Survey of the Rocky Mountain
818 Region. Washington, DC: U.S. Department of the Interior, 1877.

819 Gorelov, S.K., Drenev, N.V., Mescheryakov Y.A., Tikanov, N.A. and Fridland, V.M.: Planation surfaces of the USSR.
820 *Geomorph.*, 1, 18–29, 1970.

821 Granger, D.E., Kirchner, J.W. and Finkel, R.C.: Quaternary downcutting rate of the New River, Virginia, measured from
822 differential decay of cosmogenic ²⁶Al and ¹⁰Be in cave-deposited alluvium. *Geol.*, 25, 107-110, doi: 10.1130/0091-
823 7613(1997)025<0107:QDROTN>2.3.CO;2, 1997.

824 Green, P.F., Duddy, I.R., Japsen P., Bonow, J.M. and Malan, J.A.: Post-breakup burial and exhumation of the southern margin
825 of Africa. *Basin Res.*, 29, 96 – 127, doi: 10.1111/bre.12167, 2016.

826 Guillocheau, F., Chelalou, R., Linol, B., Dauteuil, O., Robin, C., Mvondo, F., Callec, Y. and Colin, J.P.: Cenozoic landscape
827 evolution in and around the Congo Basin: constraints from sediments and planation surfaces. In: de Wit, M.J., Guillocheau, F.
828 and de Wit, M.C.J. (eds) *Geology and Resource Potential of the Congo Basin. Regional Geology Reviews*, Springer, 271-313,
829 2015.

830 Guillocheau, F., Simon, B., Baby, G., Bessin, P., Robin, C. and Dauteuil, O.: Planation surfaces as a record of mantle dynamics:
831 the case example of Africa. *Gondwana Res.*, 53, 82-98, doi: 10.1016/j.gr.2017.05.015, 2018.

832 Gunnell, Y., Braucher, R., Bourles, D. and André, G.: Quantitative and qualitative insights into bedrock landform erosion on
833 the South Indian craton using cosmogenic nuclides and apatite fission tracks. *Geol. Soc. Am. Bull.*, 119, 576-585, doi:
834 10.1130/B25945.1, 2007.

835 Hagedorn, J.: Silcretes in the Western Little Karoo and their relation to geomorphology and palaeoecology: *Palaeoecol. of*
836 *Afr.*, 19, 371–375, 1988.

837 [Hansma, J., Tohver, E., Schrank, C., Jourdan, F. and Adams, D., 2016. The timing of the Cape Orogeny: New ⁴⁰Ar/³⁹Ar age](#)
838 [constraints on deformation and cooling of the Cape Fold Belt, South Africa. *Gondwana Res.*, 32, 122-137.](#)
839 [doi.org/10.1016/j.gr.2015.02.005, 2016.](#)

840 Helgren, D.M. and Butzer, K.W.: Paleosols of the southern Cape Coast, South Africa: implications for laterite definition,
841 genesis, and age. *Geograph. Rev.*, 67, 430-445, doi: 10.2307/213626, 1977.

842 Hein, A.S., Hulton, N.R., Dunai, T.J., Schnabel, C., Kaplan, M.R., Naylor, M. and Xu, S.: Middle Pleistocene glaciation in
843 Patagonia dated by cosmogenic-nuclide measurements on outwash gravels. *EPSL*, 286, 184-197, doi:
844 10.1016/j.epsl.2009.06.026, 2009.

845 Hirsch, K.K., Scheck-Wenderoth, M., van Wees, J.D., Kuhlmann, G. and Paton, D.A.: Tectonic subsidence history and thermal
846 evolution of the Orange Basin. *Mar. Petrol. Geol.*, 27, 565-584, doi: 10.1016/j.marpetgeo.2009.06.009, 2010.

847 Howard, A.D. 1942. Pediment passes and the pediment problem. US Coast and Geodetic Survey, 1942.

848 Jackson J., Ritz, J.F., Siame, L., Raisbeck, G., Yiou, F., Norris, R., Youngson, J. and Bennett, E.: Fault growth and landscape
849 development rates in Otago, New Zealand, using in situ cosmogenic ¹⁰ Be. *EPSL*, 195, 185-193, doi: 10.1016/S0012-
850 821X(01)00583-0, 2002.

851 [Johnson, M.R., Van Vuuren, C.J., Hegenberger, W.F., Key, R. and Show, U.: Stratigraphy of the Karoo Supergroup in southern](#)
852 [Africa: an overview. *J. African Earth Sci.*, 23, doi.org/10.1016/S0899-5362\(96\)00048-6, 1995.](#)

853 Jerolmack, D.J., Paola, C.: Shredding of environmental signals by sediment transport. *Geophys. Res. Lett.*, 37, L19401., doi:
854 10.1029/2010GL044638, 2010.

855 Kesel, R.H.: Some aspects of the geomorphology of inselbergs in central Arizona, USA. *Z. Geomorph.*, 21, 119–46, 1977.

856 Keen-Zebert, A., Tooth, S. and Stuart, F.M.: Cosmogenic ³He measurements provide insight into lithologic controls on
857 bedrock channel incision: examples from the South African interior. *J. Geol.*, 124, 423-434, doi: 10.1086/685506, 2016.

858 King, L.C.: On the ages of African land-surfaces. *Quart. J. Geol. Soc.*, 104: 439-45, doi: 10.1144/GSL.JGS.1948.104.01-04.20,
859 1948.

860 King, L.C.: The pediment landform: some current problems. *Geol. Mag.*, 86, 245-250, doi: 10.1017/S0016756800074665,
861 1949.

862 King, L.C.: The geology of the Makapan and other caves. *Trans. Royal Soc. S. Afr.*, 33: 121-151, doi:
863 10.1080/00359195109519881, 1951.

864 King, L.C.: Canons of landscape evolution. *Geol. Soc. Am. Bull.*, 64, 721-752, doi: 10.1130/0016-
865 7606(1953)64[721:COLE]2.0.CO;2, 1953.

866 King, L.C.: Pediplanation and isostasy: an example from South Africa. *Quart. J. Geol. Soc.*, 111, 353-359, doi:
867 10.1144/GSL.JGS.1955.111.01-04.18, 1955.

868 King, L.C. 1956a. A geomorphological comparison between Eastern Brazil and Africa (Central and Southern). *Quart. J. Geol.*
869 *Soc.*, 112, 445–474, doi: 10.1144/GSL.JGS.1956.112.01-04.2, 1956a.

870 King, L.C. 1956b. A geomorfologia do Brasil oriental. *Rev. Bras. Geog.* 18,186–263, 1956b.

871 King, L.C. South African scenery. A textbook of geomorphology. 308 pp, 1963.

872 Kounov, A., Niedermann, S., de Wit, M.J., Viola, G., Andreoli, M. and Erzinger, J.: Present denudation rates at selected
873 sections of the South African escarpment and the elevated continental interior based on cosmogenic ³He and ²¹Ne. *S. Afri. J.*
874 *Geol.* 110, 235-248, doi: 10.2113/gssajg.110.2-3.235, 2007.

875 Kounov, A., Viola, G., De Wit, M. and Andreoli, M.A.G.: Denudation along the Atlantic passive margin: new insights from
876 apatite fission-track analysis on the western coast of South Africa. *Geol. Soc. London, Sp. Pub.*: 324, 287-306, doi:
877 10.1144/SP324.19, 2009.

878 Kounov, A., Niedermann, S., de Wit, M.J., Codilean, A.T., Viola, G., Andreoli, M. and Christl, M.: Cosmogenic ²¹Ne and
879 ¹⁰Be reveal a more than 2 Ma Alluvial Fan Flanking the Cape Mountains, South Africa. *S. Afr. J. Geol.*, 118, 129-144, doi:
880 10.2113/gssajg.118.2.129, 2015.

881 Kubik, P.W. and Christl, M.: ¹⁰Be and ²⁶Al measurements at the Zurich 6 MV Tandem AMS facility. *Nucl. Instrum. Methods*
882 *in Phys. Res. Section B*, 268, 880–883, doi: 10.1016/j.nimb.2009.10.054, 2010.

883 Lawson, A.C.: The epigene profiles of the desert. *Uni. California Dept. Geol. Bull.*, 9, 23–48, 1915.

884 Lidmar-Bergström, K.: Exhumed cretaceous landforms in south Sweden. *Z. Geomorph.: Supp. Band* 72, 21–40, 1988.

885 Lustig, L.K.: Trend surface analysis of the Basin and Range province, and some geomorphic implications. *US Geol. Surv.*
886 *Profess. Paper* 500-D, 1969.

887 Marker, M.E. and Holmes, P.J.: Laterisation on limestones of the Tertiary Wankoe Formation and its relationship to the African
888 Surface, southern Cape, South Africa. *Catena*, 38, 1-21, doi: 10.1016/S0341-8162(99)00066-1, 1999.

889 Marker ME, Holmes PJ. 2005. Landscape evolution and landscape sensitivity: the case of the southern Cape. *South African*
890 *Journal of Science*: 101, 53 - 60.

891 Marker, M.E., McFarlane, M.J. and Wormald, R.J.: A laterite profile near Albertinia, Southern Cape, South Africa: its
892 significance in the evolution of the African Surface. *S. Afr. J. Geol.*, 105, 67-74, doi: 10.2113/1050067, 2002.

893 Margerison, H.R., Phillips, W.M., Stuart, F.M. and Sugden, D.E.: Cosmogenic ³He concentrations in ancient flood deposits
894 from the Coombs Hills, northern Dry Valleys, East Antarctica: interpreting exposure ages and erosion rates. *EPSL*, 230, 163-
895 175, doi: 10.1016/j.epsl.2004.11.007, 2005.

896 Midgley, G.F., Hannah, L., Millar, D., Thuiller, W. and Booth, A.: Developing regional and species-level assessments of
897 climate change impacts on biodiversity in the Cape Floristic Region. *Bio. Cons.*, 112, 87-97, doi: 10.1016/S0006-
898 3207(02)00414-7, 2003.

899 Moore, A., Blenkinsop, T. and Cotterill, F.W.: Southern African topography and erosion history: plumes or plate tectonics?
900 *Terra Nova*: 21, 310-315, doi: 10.1111/j.1365-3121.2009.00887.x, 2009.

901 Mountain, E.D.: Grahamstown peneplain. *Trans. Geol. Soc. S Afr.*, 83, 47-53, 1980.

902 Norton, K.P. and Vanacker, V.: Effects of terrain smoothing on topographic shielding correction factors for cosmogenic
903 nuclide-derived estimates of basin-averaged denudation rates. *ESPL*, 34, 145-154, doi: 10.1002/esp.1700, 2009.

904 Nyblade, A.A. and Robinson, S.W.: The african superswell. *Geophys. Res. Lett.*, 21, 765-768, doi: 10.1029/94GL00631, 1994.

905 Ollier, C.: *Ancient landscapes*. Belhaven Press, London/New York, 233 pp, 1991.

906 Ollier, C. and Pain, C.: *The origin of mountains*. Routledge, London/New York, 345 pp, 2000.

907 Ouimet, W.B., Whipple, K.X., Crosby, B.T., Johnson, J.P. and Schildgen, T.F.: Epigenetic gorges in fluvial landscapes. *ESPL*,
908 33, 1993-2009, doi: 10.1002/esp.1650, 2008.

909 Owen, L.A., Finkel, R.C., Barnard, P.L., Haizhou, M., Asahi, K., Caffee, M.W. and Derbyshire, E.: Climatic and topographic
910 controls on the style and timing of Late Quaternary glaciation throughout Tibet and the Himalaya defined by ¹⁰Be cosmogenic
911 radionuclide surface exposure dating. *Quat. Sci. Rev.*, 24, 1391-1411, doi: 10.1016/j.quascirev.2004.10.014, 2005.

912 Paige, S.: Rock-cut surfaces in the desert regions. *J. Geol.*, 20, 442-50, 1912.

913 Panario, D., Gutiérrez, O., Sánchez Bettucci, L., Peel, E., Oyhançabal, P., Rabassa, J.: Ancient landscapes of Uruguay. In:
914 Rabassa, J. and Ollier, C. (Eds.) *Gondwana landscapes in southern South America*, pp. 161-199, 2014.

915 Parsons, A.J. and Abrahams, A.D.: Mountain mass denudation and piedmont formation in the Mojave and Sonoran Deserts.
916 *Am. J. Sci.*, 284, 255-71, 1984.

917 Partridge, T.C.: Cainozoic environmental change in southern Africa, with special emphasis on the last 200 000 years. *Prog.*
918 *Phys. Geog.*, 21, 3-22, doi: 10.1177/030913339702100102, 1997.

919 Partridge, T.C. 1998. Of diamonds, dinosaurs and diastrophism: 150 million years of landscape evolution in southern Africa.
920 *South African Journal of Geology*: 101, 165-184.

921 Partridge, T.C.: Evolution of Landscapes. In: Cowling, R.M., Richardson, D.M. and Pierce, S.M. (eds). Vegetation of southern
922 Africa. Cambridge University Press, pp. 1-20, 1999.

923 Partridge, T.C. and Maud, R.R.: Geomorphic evolution of southern Africa since the Mesozoic. *S. Afr. J. of Geol.*, 90, 179-
924 208, 1987.

925 Partridge, T.C. and Maud, R.R. Macro-scale geomorphic evolution of southern Africa. In Partridge T.C. and Maud, R.R.M.
926 (eds) *The Cenozoic of southern Africa*. Oxford University Press. pp. 3 – 18, 2000.

927 Paton, D.A.: Influence of crustal heterogeneity on normal fault dimensions and evolution: southern South Africa extensional
928 system. *J. Struct. Geol.*, 28, 868-886, doi: 10.1016/j.jsg.2006.01.006, 2006.

929 Peulvast, J.P. and Bétard F.: A history of basin inversion, scarp retreat and shallow denudation: The Araripe basin as a keystone
930 for understanding long-term landscape evolution in NE Brazil. *Geomorph.*, 233, 20-40, doi: 10.1016/j.geomorph.2014.10.009,
931 2015.

932 Portenga, E.W. and Bierman, P.R.: Understanding Earth's eroding surface with 10 Be. *GSA Today*: 21, 4-10, doi:
933 10.1130/G111A.1, 2011.

934 Rich, J.L.: Origin and evolution of rock fans and pediments. *Bull. Geol. Soc. Am.*, 46, 999–1024, doi: 10.1130/GSAB-46-999,
935 2935, 1935.

936 Richardson, J.C., Hodgson, D.M., Wilson, A., Carrivick, J.L. and Lang A.: Testing the applicability of morphometric
937 characterisation in discordant catchments to ancient landscapes: A case study from southern Africa. *Geomorph.*, 201, 162-176,
938 doi: 10.1016/j.geomorph.2016.02.026, 2016.

939 Richardson, J.C., Hodgson, D.M., Paton, D., Craven, B., Rawcliffe, A. and Lang, A.: Where is my sink? Reconstruction of
940 landscape development in southwestern Africa since the Late Jurassic. *Gondwana Res.*: 45, 43-64, doi:
941 10.1016/j.gr.2017.01.004, 2017.

942 Rogers, C.A.: The geological history of the Gouritz River system. *Trans. S. Afri. Phil. Soc.*, 14, 375-384, 1903.

943 Romans, B.W., Castelltort, S., Covault, J.A., Fildani, A. and Walsh, J.P.: Environmental signal propagation in sedimentary
944 systems across timescales. *Earth-Sci. Rev.*: 153: 7-29, doi: 10.1016/j.earscirev.2015.07.012, 2016.

945 Ruzkiczay-Rüdiger, Z., Braucher, R., Csillag, G., Fodor, L.I., Dunai, T.J., Bada, G., Bourlés, D. and Müller, P.: Dating
946 Pleistocene aeolian landforms in Hungary, Central Europe, using in situ produced cosmogenic 10Be. *Quat. Geochron.*, 6, 515-
947 529, doi: 10.1016/j.quageo.2011.06.001, 2011.

948 Scharf, T.E., Codilean, A.T., de Wit, M., Jansen, J.D., Kubik, P.W.: Strong rocks sustain ancient postorogenic topography in
949 southern Africa. *Geol.*, 41, 331-334, doi: 10.1130/G33806.1, 2013.

950 Sharp, R.P.: Geomorphology of the Ruby–East Humboldt Range, Nevada. *Bull. Geol. Soc. Am.*, 51, 337–72, doi:
951 10.1130/GSAB-51-337, 1940.

952 Sømme, T.O., Piper, D.J., Deptuck, M.E. and Helland-Hansen, W.: Linking onshore–offshore sediment dispersal in the Golo
953 source-to-sink system (Corsica, France) during the Late Quaternary. *J. Sed. Res.*: 81, 118-137, doi: 10.2110/jsr.2011.11, 2011

954 Sonibare, W.A., Sippel, J., Scheck-Wenderoth, M. and Mikeš, D.: Crust-scale 3D model of the Western Bredasdorp Basin
955 (Southern South Africa): data-based insights from combined isostatic and 3D gravity modelling. *Basin Res.*, 27, 125-151, doi:
956 10.1111/bre.12064, 2015.

957 Spikings, A.L., Hodgson, D.M., Paton, D.A. and Spychala, Y.T.: Palinspastic restoration of an exhumed deep-water system:
958 a workflow to improve paleogeographic reconstructions. *Interpretation*, 3, SAA71-SAA87, doi: 10.1190/INT-2015-0015.1,
959 2015

960 Stanley, J.R., Braun, J., Baby, G., Guillocheau, F., Robin, C., Flowers, R.M., Brown, R., Wildman, M. and Beucher, R.:
961 Constraining plateau uplift in southern Africa by combining thermochronology, sediment flux, topography, and landscape
962 evolution modeling. *J. Geophys. Res.: Solid Earth*, 126(7), p.e2020JB021243, doi: 10.1029/2020JB021243, 2021

963 Summerfield, M.A.: Silcrete as a palaeoclimatic indicator: evidence from southern Africa. *Palaeo.*, 41, 65-
964 79, doi: 10.1016/0031-0182(83)90076-7, 1983.

965 Tankard, A., Welsink, H., Aukes, P., Newton, R. and Stettler, E.: Tectonic evolution of the Cape and Karoo basins of South
966 Africa. *Mar. Pet. Geol.*, 26, 1379-1412, doi: 10.1016/j.marpetgeo.2009.01.022, 2009.

967 Tinker, J., De Wit, M. and Brown, R.: Mesozoic exhumation of the southern Cape, South Africa, quantified using apatite
968 fission track thermochronology. *Tectonophysics*, 455, 77-93, doi: 10.1016/j.tecto.2007.10.009, 2008a.

969 Tinker J., de Wit, M. and Brown, R.: Linking source and sink: evaluating the balance between onshore erosion and offshore
970 sediment accumulation since Gondwana break-up, South Africa. *Tectonophysics*, 455, 94-103, doi: 10.1016/j.tecto.2007.11.040,
971 2008b.

972 Twidale, C.R.: *Ancient Australian Landscapes*. Rosenberg Pub Pty Limited, 144 pp, 2007a.

973 Twidale, C.R.: Bornhardts and associated fracture patterns. *Rev. As. Geol. Arg.*, 62, 139–153, 2007b.

974 Valetton, I.: Palaeoenvironment of lateritic bauxites with vertical and lateral differentiation. *Geol. Soc. London Sp. Pub.*, 11,
975 77–90, doi: 10.1144/GSL.SP.1983.011.01.10, 1983.

976 Vandermaelen, N., Beerten, K., Clapuyt, F., Christl, M. and Vanacker, V.: Constraining the aggradation mode of Pleistocene
977 river deposits based on cosmogenic radionuclide depth profiles and numerical modelling. [Geochronology-Dis., 2022, 1-314](#),
978 [713-730](#), doi: 10.5194/gchron-4-713-2022, 2022.

979 Vanacker V., von Blanckenburg, F., Hewawasam, T. and Kubik, P.W.: Constraining landscape development of the Sri Lankan
980 escarpment with cosmogenic nuclides in river sediment, *EPSL*, 253, 402-414, doi: 10.1016/j.epsl.2006.11.003, 2007.

981 Vanacker, V., von Blanckenburg, F., Govers, G., Molina, A., Campforts, B. and Kubik, P.W.: Transient river response,
982 captured by channel steepness and its concavity. *Geomorph.*, 228, 234-243, doi: 10.1016/j.geomorph.2014.09.013, 2015.

983 van der Beek, P., Summerfield, M.A., Braun, J., Brown, R.W. and Fleming A.: Modeling postbreakup landscape development
984 and denudational history across the southeast African (Drakensberg Escarpment) margin. *J. Geophys. Res.: Solid Earth*: 107
985 (B12), doi: 10.1029/2001JB000744, 2002.

986 van der Wateren, F.M. and Dunai, T.J.: Late Neogene passive margin denudation history—cosmogenic isotope measurements
987 from the central Namib desert. *Glob. and Planet. Change*, 30, 271-307, doi: 10.1016/S0921-8181(01)00104-7, 2001.

988 van Niekerk, H.S., Beukes, N.J. and Gutzmer, J.: Post-Gondwana pedogenic ferromanganese deposits, ancient soil profiles,
989 African land surfaces and palaeoclimatic change on the Highveld of South Africa. *J. Afr. Earth Sci.*, 29, 761-781, doi:
990 10.1016/S0899-5362(99)00128-1, 1999.

991 Vermeesch, P.: CosmoCalc: An Excel add-in for cosmogenic nuclide calculations. *Geochem., Geophys., Geosyst.*: 8,
992 doi:10.1029/2006GC001530, 2007

993 von Blanckenburg F., Belshaw, N. and O'Nions, R.: Separation of ⁹Be and cosmogenic¹⁰Be from environmental materials
994 and SIMS isotope dilution analysis. *Chem. Geol.*, 129, 93–99, doi: 10.1016/0009-2541(95)00157-3, 1996.

995 von Blanckenburg, F., Hewawasam, T., Kubik, P.W.: Cosmogenic nuclide evidence for low weathering and denudation in the
996 wet, tropical highlands of Sri Lanka. *J. Geophys. Res.: Earth Surface*: 109, F3, doi: 10.1029/2003JF000049, 2004.

997 Widdowson, M.: Laterite and Ferricrete. In: Nash DJ, McLaren SJ. (eds.) *Geochemical Sediments and Landscapes*. Oxford,
998 UK: Wiley-Blackwell, pp. 46–94, 2007.

999 Wildman, M., Brown, R., Watkins, R., Carter, A., Gleadow, A. and Summerfield, M.: Post break-up tectonic inversion across
1000 the southwestern cape of South Africa: new insights from apatite and zircon fission track thermochronometry. *Tectonophys.*,
1001 654, 30–55, doi: 10.1016/j.tecto.2015.04.012, 2015.

1002 Wildman, M., Brown, R., Beucher, R., Persano, C., Stuart, F., Gallagher, K., Schwanethal, J. and Carter, A.: The chronology
1003 and tectonic style of landscape evolution along the elevated Atlantic continental margin of South Africa resolved by joint
1004 apatite fission track and (U-Th-Sm)/He thermochronology. *Tectonics*: 35, doi: 10.1002/2015TC004042, 2016.

1005 Wildman, M., Brown, R., Persano, C., Beucher, R., Stuart, F.M., Mackintosh, V., Gallagher, K., Schwanethal, J. and Carter,
1006 A.: Contrasting Mesozoic evolution across the boundary between on and off craton regions of the South African plateau
1007 inferred from apatite fission track and (U-Th-Sm)/He thermochronology. *J. Geophys. Res.: Solid Earth*, 122(2), pp.1517-1547,
1008 doi: 10.1002/2016JB013478, 2017.

1009 Willenbring, J.K. and von Blanckenburg, F.: Long-term stability of global erosion rates and weathering during late-Cenozoic
1010 cooling. *Nature*: 465, 211-214, 2010.

1011 Wittmann H., von Blanckenburg, F., Kruesmann, T., Norton, K.P. and Kubik, P.W.: Relation between rock uplift and
1012 denudation from cosmogenic nuclides in river sediment in the Central Alps of Switzerland. *J. Geophys. Res.: Earth Surface*:
1013 112 (F4), doi: 10.1029/2006JF000729, 2007.

1014 Wittmann H., Von Blanckenburg, F., Guyot, J.L., Maurice, L., Kubik, P.W.: From source to sink: Preserving the cosmogenic
1015 ¹⁰Be-derived denudation rate signal of the Bolivian Andes in sediment of the Beni and Mamoré foreland basins. *EPSL*, 288,
1016 463-474, doi: 10.1016/j.epsl.2009.10.008, 2009.

1017
1018
1019